



Kent Academic Repository

Comsa, Iulia M., Bekinschtein, Tristan A. and Chennu, Srivas (2018) *Transient topographical dynamics of the electroencephalogram predict brain connectivity and behavioural responsiveness during drowsiness*. *Brain Topography*, 32 . pp. 315-331. ISSN 0896-0267.

Downloaded from

<https://kar.kent.ac.uk/70355/> The University of Kent's Academic Repository KAR

The version of record is available from

<https://doi.org/10.1007/s10548-018-0689-9>

This document version

Author's Accepted Manuscript

DOI for this version

Licence for this version

UNSPECIFIED

Additional information

Versions of research works

Versions of Record

If this version is the version of record, it is the same as the published version available on the publisher's web site. Cite as the published version.

Author Accepted Manuscripts

If this document is identified as the Author Accepted Manuscript it is the version after peer review but before type setting, copy editing or publisher branding. Cite as Surname, Initial. (Year) 'Title of article'. To be published in **Title of Journal**, Volume and issue numbers [peer-reviewed accepted version]. Available at: DOI or URL (Accessed: date).

Enquiries

If you have questions about this document contact ResearchSupport@kent.ac.uk. Please include the URL of the record in KAR. If you believe that your, or a third party's rights have been compromised through this document please see our [Take Down policy](https://www.kent.ac.uk/guides/kar-the-kent-academic-repository#policies) (available from <https://www.kent.ac.uk/guides/kar-the-kent-academic-repository#policies>).

[Click here to view linked References](#)

1 **Transient topographical dynamics of the electroencephalogram predict**
2 **brain connectivity and behavioural responsiveness during drowsiness**

3 Iulia M. Comsa¹, Tristan A. Bekinschtein², Srivas Chennu^{3, 1, *}

4 ¹ Department of Clinical Neurosciences, University of Cambridge, United Kingdom

5 ² Department of Psychology, University of Cambridge, United Kingdom

6 ³ School of Computing, University of Kent, United Kingdom

7 * Correspondence: Srivas Chennu, Medway Building, Chatham Maritime ME4 4AG, United
8 Kingdom; sc785@kent.ac.uk; +44 1634 88 88 17; ORCID: 0000-0002-6840-2941

9

10 **Abstract**

11 As we fall sleep, our brain traverses a series of gradual changes at physiological, behavioural and
12 cognitive levels, which are not yet fully understood. The loss of responsiveness is a critical event in
13 the transition from wakefulness to sleep. Here we seek to understand the electrophysiological
14 signatures that reflect the loss of capacity to respond to external stimuli during drowsiness using two
15 complementary methods: spectral connectivity and EEG microstates. Furthermore, we integrate
16 these two methods for the first time by investigating the connectivity patterns captured during
17 individual microstate lifetimes. While participants performed an auditory semantic classification
18 task, we allowed them to become drowsy and unresponsive. As they stopped responding to the
19 stimuli, we report the breakdown of alpha networks and the emergence of theta connectivity.
20 Further, we show that the temporal dynamics of all canonical EEG microstates slow down during
21 unresponsiveness. We identify a specific microstate (D) whose occurrence and duration are
22 prominently increased during this period. Employing machine learning, we show that the temporal
23 properties of microstate D, particularly its prolonged duration, predicts the response likelihood to
24 individual stimuli. Finally, we find a novel relationship between microstates and brain networks as
25 we show that microstate D uniquely indexes significantly stronger theta connectivity during
26 unresponsiveness. Our findings demonstrate that the transition to unconsciousness is not linear, but
27 rather consists of an interplay between transient brain networks reflecting different degrees of sleep
28 depth.

29 **Keywords:** drowsiness; responsiveness; EEG microstates; brain connectivity

30 **Author summary**

31 How do we lose responsiveness as we fall asleep? As we become sleepy, our ability to react to
32 external stimuli disappears gradually. Here we sought to understand the rapid fluctuations in brain
33 electrical activity that predict the loss of responsiveness as participants fell asleep while performing
34 a word classification task. We analysed the patterns of connectivity between anterior and posterior
35 brain regions observed during wakefulness in alpha band and showed that this connectivity shifted
36 to slower theta frequencies as participants became unresponsive. We also investigated the dynamics
37 of brain electrical microstates, which represent an alphabet of quasi-stable global brain states with
38 lifetimes of 10-100 milliseconds, and found that the temporal dynamics of microstates slowed down
39 when participants became unresponsive. Using machine learning, we further showed that
40 microstate dynamics prior to a stimulus predict whether subjects will respond to it. We integrated
41 microstates and connectivity for the first time to show that a specific microstate captures
42 connectivity patterns correlated with unresponsiveness during this transition. We conclude that
43 falling asleep is accompanied by a millisecond-level interplay between distinct brain networks, and
44 suggest a renewed focus on fine-grained temporal scales in the study of transitions between levels
45 of consciousness.

46 Introduction

47 As we fall asleep, our brain traverses a series of changes which accompany the loss of sensory
48 awareness and responsiveness to the external world. Despite the subjective ability to classify
49 retrospectively one's own state as "awake" or "asleep" (Hori et al., 1994), research continues to
50 unravel the gradual transitions happening at behavioural (Ogilvie and Wilkinson, 1984), cellular
51 (Steriade et al., 1993), physiological (Prerau et al., 2014) and cognitive (Goupil and Bekinschtein,
52 2012) level, starting with early drowsiness and continuing into the deep stages of sleep (Ogilvie,
53 2001). Characterising these transitions and linking across physiological levels is an important step in
54 the modern attempt to understand access-consciousness (Block, 1996; Koch et al., 2016) and its
55 fluctuations in natural, pathological and pharmacological alterations: sleep (Hobson and Pace-
56 Schott, 2002), disorders of consciousness (Giacino et al., 2014), sedation and anaesthesia (Alkire et
57 al., 2008).

58 The transition from wakefulness to sleep involves a progressive and sometimes nonlinear loss of
59 responsiveness to external stimuli (Ogilvie and Wilkinson, 1984). Behavioural unresponsiveness does
60 not immediately imply unconsciousness (Overgaard and Overgaard, 2011; Sanders et al., 2013).
61 However, from the perspective of levels of consciousness (Laureys, 2005), the capacity to respond to
62 external stimuli offers an objective measurement in the process of transition between full
63 wakefulness and sleep-induced unconsciousness. The question of how we stop responding to stimuli
64 during drowsiness is related to, but distinct from an investigation of the stages of sleep
65 conventionally defined by specific electrophysiological grapho-elements (Iber et al., 2007; Ogilvie,
66 2001). Indeed, the loss of responsiveness is and distributed across sleep stages: one study found a
67 rate of unresponsiveness of 28% in stage 1, 76% in stage 2, and 95% in stage 3 of sleep (Ogilvie and
68 Wilkinson, 1984). Here, we are specifically interested in the neural markers that predict our inability
69 to respond as we drift to sleep.

70 A traditional approach for investigating this question is to look at the changes in EEG spectral power
71 and connectivity, which have been shown to vary across levels of consciousness. During relaxed
72 wakefulness, the EEG of most human subjects is characterised by trains of alpha waves, at around
73 10 Hz, originating from central-posterior cortical areas (Barry et al., 2007; De Gennaro et al., 2016;
74 Niedermeyer, 2005a). During the early onset of sleep, these alpha oscillations disappear and an
75 alpha rhythm with a different cortical origin (Broughton and Hasan, 1995) emerges in anterior
76 regions (Tanaka et al., 1997), while theta power increases, particularly in central regions (Badia et al.,
77 1994; Niedermeyer, 2005b; Ogilvie, 2001; Wright et al., 1995). Similarly, long-range alpha

1
2
3
4
5
6
7
8
9
10
11
12
13
14
15
16
17
18
19
20
21
22
23
24
25
26
27
28
29
30
31
32
33
34
35
36
37
38
39
40
41
42
43
44
45
46
47
48
49
50
51
52
53
54
55
56
57
58
59
60
61
62
63
64
65

78 connectivity disintegrates at the onset of sleep, while lower-frequency theta and delta connectivity
79 increases (Tanaka et al., 2000, 1998; Wright et al., 1995). Several power and connectivity patterns
80 have been associated with the loss of consciousness, sometimes specifically with the loss of
81 responsiveness, such as the anteriorisation of alpha power and connectivity in EEG, which has been
82 described in drug-induced loss of responsiveness (Chennu et al., 2016), and frontoparietal
83 connectivity in fMRI, which has been proposed as a key signature of consciousness (Laureys, 2005)
84 and linked to external awareness (Vanhaudenhuyse et al., 2011). In EEG, the disruption of
85 connectivity between frontal and parietal electrodes at alpha (8-12 Hz) frequencies has been shown
86 to occur in disorders of consciousness (Chennu et al., 2014) and sedation (Chennu et al., 2016).
87 Although it is still debated whether these are signatures of conscious processing or of processes that
88 almost invariably accompany it (Farooqui and Manly, 2017), brain connectivity patterns currently
89 provide, in practice, useful insights into the transitions between levels of consciousness.

90 Another method that can be employed to investigate the rapidly changing global state of the brain is
91 that of EEG microstates. A microstate represents a quasi-stable spatial topography of electric field on
92 the scalp (Lehmann, 1990, 1971; Lehmann et al., 1987). The conventional method of analysing
93 microstates in a dataset involves running an unsupervised clustering algorithm on a set of EEG
94 topographies of highest variance, followed by labelling of all EEG samples based on the similarity
95 with the four obtained topographies (Murray et al., 2008; Pasqual-Marqui et al., 1995). Four
96 consistent (Khanna et al., 2014) EEG microstate topographies have been identified in a large
97 population of healthy subjects of all ages during resting-state wakefulness (Koenig et al., 2002) and
98 different microstates have been correlated with different cognitive modalities (Lehmann et al., 2010;
99 Milz et al., 2015; Seitzman et al., 2016), but also with mental disorders, such as narcolepsy (Kuhn et
100 al., 2015). A resting-state study of sleep (Brodbeck et al., 2012) identified four EEG microstate
101 topographies in all stages of sleep nearly identical to those of wakefulness, but occurring with
102 altered temporal parameters. Notably, increased microstate duration was associated with deeper
103 sleep. On the contrary, a different study (Cantero et al., 1999) reported a shorter duration of
104 microstates and suggested a larger repertoire of brain states during the hypnagogic period.
105 Microstates are thought to reflect momentary, global, synchronised (Koenig et al., 2005) networks of
106 the brain, reflecting building blocks of large-scale cognitive processing required for the continuous
107 stream of consciousness (Lehmann, 1990). The neural sources underlying microstates are still being
108 explored (Britz et al., 2010; Milz et al., 2017; Pascual-Marqui et al., 2014). Still, the dynamics of the
109 sequence of microstates itself can be seen as a “syntax” of neural activity that is in and of itself an

110 informative tool for modelling and understanding the rapidly-fluctuating global dynamics of the
111 brain.

112 Brain connectivity and microstates hence provide complementary perspectives on the
113 neurodynamics underlying the loss of responsiveness as we fall asleep. But what is the relationship
114 between brain networks and microstates? There is evidence that transient brain networks can be
115 resolved in electrophysiological data (Baker et al., 2014; Pascual-Marqui et al., 2014; Vidaurre et al.,
116 2016), but it is an open question whether these networks co-occur with the lifetime of individual
117 microstates. We investigate for the first time how spectral connectivity and EEG microstate
118 dynamics interact as we lose responsiveness during drowsiness. We hypothesise that the spectral
119 changes occurring with the loss of responsiveness mirror those observed in the transition to sleep
120 (Ogilvie, 2001), anaesthesia (Chennu et al., 2016; Purdon et al., 2013) and in disorders of
121 consciousness (Chennu et al., 2014): namely, the disintegration of alpha networks, the loss of
122 posterior alpha power, and the emergence of lower-frequency connectivity and power. Alongside,
123 building on previous research on EEG microstate dynamics during sleep (Brodbeck et al., 2012), we
124 hypothesise similar changes in microstate dynamics accompanying the loss of responsiveness during
125 drowsiness. Finally, given that resting-state network activity is known to fluctuate at millisecond
126 level, we hypothesise that the neural changes in that occur during drowsiness underlie the dynamics
127 of both brain networks and the microstates sequence. Specifically, we investigate the possibility that
128 individual microstates co-occur with distinct transient brain networks, reflecting fleeting changes in
129 the global state of the brain during drowsiness.

130 To address these questions, we use a subset of data from a previously reported auditory
131 discrimination task where subjects became drowsy and unresponsive (Kouider et al., 2014). The task
132 involved pressing a button corresponding to the classification of the auditory stimulus into one of
133 two categories (object or animal). We obtain five minutes of data as subjects performed this task,
134 before and after the loss of responsiveness due to drowsiness. We first characterise the responsive
135 and unresponsive periods by analysing microstate-blind spectral power and connectivity changes in
136 our dataset. Next, we describe the temporal parameters of EEG microstates during responsiveness
137 and unresponsiveness. To test whether these parameters can reliably predict responsiveness to
138 individual stimuli, we apply machine learning to predict responses and misses to stimuli in our task,
139 based only on pre-stimulus microstate parameters. Finally, we investigate the brain connectivity
140 underlying each of the four canonical microstates after the loss of responsiveness and highlight a
141 previously unknown relationship between spectral connectivity and EEG microstates.

142 **Methods**

143 **Subjects**

144 Sixteen healthy, native English-speaking, right-handed young adults (mean age = 24, S.D. = 2.75; 6
145 females) were selected for this experiment out of the eighteen subjects from Experiment 1 in a
146 previous study (Kouider et al., 2014). Two subjects from this dataset were excluded by visual
147 inspection due to a failure to remain asleep for a period longer than five minutes, as assessed using
148 responsiveness to stimuli. The participants were directed to not consume stimulants like coffee and
149 to sleep 1-2 hours less than normally before the experiment. All of the subjects were assessed as
150 easy sleepers on the Epworth Sleepiness Scale (scores 7-14). The participants signed a consent form
151 and were reimbursed for their participation. The experiment was approved by the Cambridge
152 Psychology Research Ethics Committee.

153 **Experimental procedure**

154 The stimuli consisted of 96 spoken English words chosen from the CELEX lexical database (Linguistic
155 Data Consortium, University of Pennsylvania). Half of the words denoted animals and the other half
156 denoted objects. The subjects were asked to classify each stimulus in its respective category (animal
157 or object) by pressing a button. The stimuli were presented through headphones, with an average
158 distance of 8.4 seconds (minimum 6.2 seconds) between consecutive stimuli, as the subjects were
159 lying with their eyes closed in a reclining chair. To facilitate drowsiness, the task was performed in a
160 dark, acoustically and electrically shielded EEG room, and the participants were told that they could
161 fall asleep at any point during the experiment, although they were asked not to stop responding
162 deliberately while still awake.

163 **EEG data acquisition**

164 The electroencephalogram was continuously recorded at 500 samples per second from 64 Ag/AgCl
165 electrodes (NeuroScan Labs system) positioned and labelled according to the extended 10/20
166 system, with Cz as a reference and including vertical and horizontal electrooculography channels.

167 **EEG pre-processing**

168 All analyses that follow were performed using custom MATLAB scripts (The MathWorks, Inc., Natick,
169 Massachusetts, US). The EEGLAB toolbox (Delorme and Makeig, 2004) was used to facilitate data
170 pre-processing.

171 The data was filtered between 1 and 40 Hz and the full channel mean was subtracted from each
172 channel for baseline correction. The HEOG and VEOG channels were removed. An Independent
173 Component Analysis (ICA) decomposition was performed using the infomax ICA algorithm (Bell and
174 Sejnowski, 1995). Components capturing ocular or single-channel artefacts were removed from the
175 data by visual inspection and considering the correlation with the HEOG and VEOG channels. An
176 average of 11.6 (S.D. = 8.6) out of 63 components were removed per subject. Channel FT8 was
177 interpolated using spherical interpolation in all subjects as it was noisy in most recordings. Finally,
178 channels were re-referenced offline to the common average.

179 **Data segmentation**

180 We classified responsive and unresponsive periods by inspecting the sequence of hits and misses to
181 individual stimuli. We used a liberal window of 6 seconds to allow for a response to a stimulus,
182 regardless of its correctness. A lack of response within 6 seconds was marked as a miss. The choice
183 of a 6-second window for responsiveness was based on our own pilot studies, where we investigated
184 the longest interval that subjects would make a response during drowsiness in a go task. However,
185 note that most reaction times were below 3 seconds (Fig. 1) and the reaction times increased
186 gradually and later in the task, indicating an increase in drowsiness. This was also established in a
187 previous study on the same data (Kouider et al., 2014).

188 For balance across participants and the two behavioural states, a total of five minutes of
189 responsiveness and five minutes of unresponsiveness were extracted from each recording (150000
190 samples per state, per recording), as shown in Fig. 1. The responsiveness period was taken as the
191 first 0.5 to 5.5 minutes of data in each recording, acquired immediately after the experiment began
192 and the participants were still alert and wakeful. This was confirmed by checking that the large
193 majority of the stimuli were followed by responses during this period; a very small number of
194 occasional misses occurred in more than half of the participants during this period (e.g., due to
195 unfamiliarity with the task), but they were not contiguous. Then, a period of unresponsiveness was
196 selected by visual inspection of the hits and misses after the end of the responsiveness period, with
197 the aim to find a five-minute interval consisting of as many misses as possible. If a response was
198 present during the period labelled as unresponsiveness, the 10 seconds preceding and following the
199 corresponding stimulus were excluded.

200 **Microstate topographies**

1
2
3 201 The idea of electric microstates of the brain comes from the observation that the topography of the
4
5 202 electric field recorded by EEG over the scalp does not fluctuate randomly, but is instead comprised
6
7 203 of short periods of stability (Lehmann, 1971). Four canonical microstates (Koenig et al., 2002),
8
9 204 conventionally labelled A, B, C and D, have been shown to be consistent across recording sessions
10
11 205 (Khanna et al., 2014) and have been repeatedly confirmed in a wide range of health conditions and
12
13 206 cognitive tasks across multiple studies (Britz et al., 2010; Brodbeck et al., 2012; Grieder et al., 2016;
14
15 207 Katayama et al., 2007; Kikuchi et al., 2011; Koenig et al., 1999; Kuhn et al., 2015; Milz et al., 2015;
16
17 208 Nishida et al., 2013; Pascual-Marqui et al., 2014; Schlegel et al., 2012; Strelets et al., 2003; Tomescu
18
19 209 et al., 2014; Van de Ville et al., 2010).

20
21 210 To compute the microstate topographies, the Global Field Power (GFP), representing the standard
22
23 211 deviation of the electrode values (Lehmann and Skrandies, 1980), was first computed at each time
24
25 212 point. As the number of GFP peaks varied across subjects and condition, we rounded down the
26
27 213 minimum number of peaks available and retained the first 5000 peaks in each condition
28
29 214 (responsiveness and unresponsiveness) from each recording.

30
31 215 The clustering algorithm was implemented in MATLAB and is presented in Box 1. The algorithm is
32
33 216 based on a variant of the method first introduced by (Lehmann et al., 1987), as described in (Murray
34
35 217 et al., 2008), and involves an unsupervised clustering of EEG samples into the specified number of
36
37 218 classes that best explain the input samples. Note that topographical similarity is computed using the
38
39 219 absolute value of the spatial correlation, and the polarity of the map is ignored, as topographies with
40
41 220 inverted polarities are considered to be produced by the same neural generators (Michel et al.,
42
43 221 2009). The maximum number of iterations was set to 1000 and the GEV delta was set to 1e-9.
44
45
46
47
48
49
50
51
52
53
54
55
56
57
58
59
60
61
62
63
64
65

Microstate clustering algorithm

Input: n average-referenced EEG samples ($n \times \text{number_of_channels}$) from GFP peaks.

Output: k maps that best characterise the data.

1. Normalize each input sample to a vector of length 1.
2. Pick k random samples as the initial maps.
3. Label each sample as $i \in \{1, \dots, k\}$, where i is the index of the map with highest absolute spatial correlation.
4. Re-compute each map i as the first principal component of each cluster of samples labelled i .
5. Compute the Global Explained Variance (GEV).
6. If GEV delta is small enough or maximum number of iterations has been reached, end; else, go to 3.

Box 1. Microstate clustering algorithm.

We initially employed a cross-validation criterion (Pasqual-Marqui et al., 1995) to determine the optimal number of microstates fitting the data, as performed in several previous studies (Brodbeck et al., 2012; Koenig et al., 1999). However, we found that the cross-validation criterion produced different results for when the number of electrodes was down-sampled from 63 to 30 (7 and 4 maps, respectively). This sensitivity of the cross-validation criterion to the number of electrodes has been documented in previous literature (Murray et al., 2008). Hence, we decided to fix the number of microstates to four, in line with previous studies that also fix this number a priori (Khanna et al., 2014; Kikuchi et al., 2007; Koenig et al., 2002; Milz et al., 2015; Schlegel et al., 2012; Strelets et al., 2003; Tomescu et al., 2014).

Microstate labelling

To obtain the sequence of EEG microstates characterising a recording, each EEG sample was individually assigned to the microstate with the highest corresponding spatial correlation. To correct for noisy assignments during polarity reversals (Koenig and Brandeis, 2016), we applied a previously-described temporal smoothing algorithm for the microstate sequence (Pasqual-Marqui et al., 1995) with parameter b set to 5, corresponding to a smoothing neighbourhood of 20ms. This parameter was chosen to be in the range of mean microstate durations found by (Gärtner et al., 2015) using a

240 model of microstate transition processes based on Markov chains (10 ms during wake, 34 ms during
241 deep sleep).

242 **Microstate properties**

243 Following the full labelling of each recording, three properties were computed for each microstate
244 per state (responsiveness and unresponsiveness) and per recording:

- 245 • The *microstate temporal coverage*, also called the *fractional occupancy*, indicating the
246 percentage of time spent in one microstate;
- 247 • The *microstate duration*, indicating the average length of continuous sequences labelled as one
248 microstate;
- 249 • The *Global Explained Variance (GEV)*, representing the amount of spatial correlation of the
250 samples with their corresponding microstate topography, normalised by the GFP of the
251 microstate topography.

252 **Statistics**

253 Interactions between microstate parameters and behavioural state (responsiveness and
254 unresponsiveness) were performed using a two-way repeated measures ANOVA (Hogg and Ledolter,
255 1987) with the microstate label and the behavioural state as factors. Sphericity was tested using
256 Mauchly's test of sphericity (Mauchly, 1940) and, where violated, was corrected using the
257 Greenhouse-Geisser procedure (Greenhouse and Geisser, 1959). The Tukey-Kramer method (Tukey,
258 1949) was used to correct for multiple comparisons. After correction, a conventional threshold of
259 $p=0.05$ was used to assess significance. Unless otherwise specified, similar statistical tests were also
260 performed for the measures that follow.

261 **Responsiveness prediction**

262 We applied machine learning classification to explore whether microstate properties identified in
263 the ongoing brain dynamics immediately preceding each auditory stimulus in the experimental trials
264 could predict the presence or absence of a response to that stimulus. Importantly, *all* trials were
265 considered for classification, both within and outside the periods labelled as responsive or
266 unresponsive for the above microstate analysis.

267 Five seconds of EEG data immediately preceding a stimulus were used to generate the features for
268 classification. We also investigated using shorter pre-stimulus time periods, down to 1 second of
269 pre-stimulus data, but we found that classification accuracy increased with a larger amount of pre-

270 stimulus data over which microstate dynamics could be more accurately estimated. At the same
271 time, the amount of pre-stimulus data was restricted by the overlap with the previous trial. Trials
272 overlapping with a response corresponding to the previous stimulus were excluded. By setting the
273 pre-stimulus window to five seconds, less than 10% of the trials were rejected due to overlap with
274 the previous trial.

275 The input features generated for classification consisted of either individual microstate parameters
276 computed during the five-second pre-stimulus period in each trial, or a combination of these
277 parameters. The parameters were those we previously characterised at the group level: namely the
278 mean duration, mean coverage, and mean GEV for each microstate separately. The classifier was
279 trained separately with the above individual and combined features. As a baseline, the theta-alpha
280 ratio was also computed for each trial as the ratio between the total power spectral density at 5-6
281 and 9.5-10.5 Hz respectively, and used as an input feature for the classifier. The classification label
282 for each trial was generated by labelling it as either as a timely response (1) or a miss (0).

283 We employed leave-one-subject-out cross-validation to test for the generalisability of the classifier's
284 performance. For this, the data was split into 16 folds, with one fold corresponding to a single
285 participant's trials. A support vector machine (SVM) (Christianini and Shawe-Taylor, 2000) with a
286 radial basis function kernel (Vert et al., 2004) was trained repeatedly by excluding one fold at the
287 time from the training set and using it as a test set. The SVM was optimised by exhaustive search to
288 use the optimal value for two parameters: the box constraint, which restricts the number of support
289 vectors, and the kernel scale, both in the range [0.001, 1000] in logarithmic steps of 10.

290 Platt's method (Platt, 1999) was used to generate class affiliation probabilities from the trained
291 classifier. These continuously varying probabilities were then used to discriminate between
292 responses and misses using both the Receiver Operator Characteristic (ROC) area under the curve
293 (AUC) (Davis and Goadrich, 2006) and the classification accuracy as the percentage of correct
294 predictions out of the total number of predictions. The classification accuracy was also computed by
295 setting the class discrimination threshold as the optimal operating point of the ROC curve and
296 calculating the percentage of correct predictions, using the threshold as a boundary between the
297 two target classes. We used Wilcoxon signed rank tests (Gibbons and Chakraborti, 2011) to probe for
298 significant differences between classification performances.

299 Spectral power and connectivity analyses

1
2
3 300 Spectral power and connectivity during responsiveness and unresponsiveness was investigated in
4
5 301 both microstate-blind and microstate-wise analyses. Before microstate-wise segmentation, the
6
7 302 power spectral density was computed at each EEG sample between 1 and 20 Hz as the absolute
8
9 303 value of the Hilbert transform (Marple, 1999) of the bandpass filtered data within windows of 0.25
10
11 304 Hz. We performed most of the analysis on 1 to 20 Hz and focused on theta and alpha power, whose
12
13 305 ratio has been shown to track the onset of sleep (Šušmáková and Krakovská, 2007) and has been
14
15 306 employed in other studies of drowsiness (Bareham et al., 2014) or impaired consciousness
16
17 307 (Lechinger et al., 2013). For each channel in each recording, the spectral power at each frequency
18
19 308 bin was divided by the sum of spectral power at all bins within 1 to 20 Hz. This ratio was then
20
21 309 multiplied by 100, thereby obtaining relative power contribution percentage at that bin.

21 310 The connectivity within each pair of channels was analysed using the Weighted Phase Lag Index
22
23 311 (WPLI) (Vinck et al., 2011), a connectivity measure based on the distribution of phase differences
24
25 312 between signals designed to correct for volume conduction, which has been previously used to
26
27 313 investigate brain connectivity during loss of consciousness (Chennu et al., 2016, 2014; Lee et al.,
28
29 314 2013). The WPLI was obtained by pooling over the Hilbert phase of each sample labelled as
30
31 315 belonging to a particular microstate (see Suppl. Fig. 1).

32
33 316 For both spectral power and connectivity, the median across channels was computed to obtain one
34
35 317 value per microstate and frequency of interest.

36
37 318 To further assess topographical changes in connectivity, two sets representing anterior (AFz, Fz, FCz,
38
39 319 AF7, AF3, F1, FC1, F3, FC3, F5, F7, AF8, AF4, F2, FC2, F4, FC4, F6, F8) and posterior (CPz, Pz, POz, Oz,
40
41 320 P1, P2, PO3, PO4, O1, O2, P3, P5, P7, P4, P6, P8, CP3, CP1, CP2, CP4) electrodes were selected for
42
43 321 analysis. Median WPLI connectivity was computed within the anterior and posterior groups
44
45 322 separately for each participant.

47 Results

49 Behavioural data

50
51
52 325 The distribution of responsiveness and reaction times over time confirmed that all the subjects were
53
54 326 responsive for a minimum of six minutes in the beginning of the experimental session and became
55
56 327 unresponsive at a later point. During the unresponsiveness period, participants predominantly
57
58 328 reached sleep stage N1, and rarely N2, as detailed in (Kouider et al., 2014). Fig. 1 shows the response

329 reaction times and the misses in each participant, in addition to the selection of data for the
330 subsequent microstate analysis. During responsive periods, most subjects had no more than one
331 miss, with a mean of 2.125% of all responses during this period being misses. The grand average of
332 reaction times during the responsive period was 1.5s (S.D. = 0.7).

333 **Spectral power and connectivity dynamics**

334 Before delving into microstate analyses, we characterised the spectral power and connectivity
335 patterns during responsive and unresponsive periods. We performed a microstate-blind analysis
336 focusing on previously reported changes related to early sleep, but also anaesthesia and disorders of
337 consciousness, including the alteration of posterior, frontal and frontoparietal connectivity within
338 and between frontal and parietal electrodes. We focused on alpha and theta frequencies, as the
339 theta-alpha ratio has been shown to be the best discriminator between wake and sleep stage 1
340 (Šušmáková and Krakovská, 2007). We confirmed that there were no significant differences in the
341 means of power and median connectivity in beta (12-30 Hz) or gamma (30-40 Hz) between the
342 responsive and unresponsive periods. Based on the peaks present in alpha and theta bands in our
343 data at 5.5 and 10 Hz (also see Fig. 6 later), we defined the spectral frequencies of interest in alpha
344 range at 9.5 to 10.5 Hz and the theta frequencies of interest at 5 to 6 Hz, for both power
345 contributions and connectivity.

346 We observed a decrease in mean alpha power contribution ($t(1,15) = 3.34$, $p = 0.0044$, Cohen's $d =$
347 0.83) and an increase in mean theta power contribution ($t(1,15) = 7.1$, $p = 3.5e^{-6}$, Cohen's $d = 1.77$)
348 going from responsiveness to unresponsiveness. As shown in Suppl. Fig. 2, we noted an alpha peak
349 in spectral power present around 10 Hz in the large majority of the participants during the
350 responsive period, which faded during the unresponsive period. Lower-frequency power in the theta
351 frequency range increased during unresponsiveness. A single notable exception was Subject 12,
352 whose alpha peak did not shift into theta range during the unresponsive period, however this
353 subject was preserved in the analysis since there was no evidence that the experiment instructions
354 were not followed. A grand average topographic plot of power at alpha and theta frequencies (Fig.
355 2A) revealed that the highest alpha power was located in the posterior area during responsiveness.
356 During unresponsiveness, theta power was highest in posterior channels.

357 Investigating connectivity in alpha and theta frequencies using the WPLI, we observed the
358 disintegration of long-range alpha band connections between frontal and parietal electrodes going
359 from responsiveness to unresponsiveness (Fig. 2B and Suppl. Fig. 3). A paired t-test confirmed that
360 the median alpha connectivity between the anterior and posterior channels was significantly higher

361 during responsiveness ($t(1, 15) = 3.4, p = 0.003, \text{Cohen's } d = 0.85$). At the same time, an overall
362 increase in median frontoparietal connectivity was observed in theta frequencies in
363 unresponsiveness, but this was not significant ($t(1, 15) = 0.4, p = 0.69, \text{Cohen's } d = 0.1$).

364 **Microstate topographies**

365 We applied the microstate clustering algorithm on the set of combined samples from the responsive
366 and unresponsive periods from each subject, in order to obtain four microstate topographies. The
367 resulting maps matched the four canonical microstate topographies commonly described in
368 literature, denoted by letters A to D (Fig. 3). A breakdown of microstate topographies obtained for
369 individual participants is also shown in Suppl. Fig. 4.

370 **Microstate parameters**

371 We investigated whether the dynamics of the rapid succession of microstates in the EEG remains the
372 same before and after the loss of responsiveness. We computed the duration, the temporal
373 coverage and the global explained variance (GEV) of each microstate during responsiveness and
374 during unresponsiveness (Fig. 4).

375 A repeated measures ANOVA with the microstate and the behavioural state (responsiveness and
376 unresponsiveness) as factors found significant interactions between microstate and behavioural
377 state in all of the three microstate parameters investigated: duration ($F_{interaction} = 16.73,$
378 $P_{interaction} = 2e^{-7}, \text{Cohen's } d = 2.11$), temporal coverage ($F_{interaction} = 13.08, P_{interaction} = 3e^{-6},$
379 $\text{Cohen's } d = 1.86$) and GEV ($F_{interaction} = 17.95, P_{interaction} = 8e^{-8}, \text{Cohen's } d = 2.18$). Further exploring the
380 simple effect of state on the parameters within each microstate, the ANOVA revealed that the
381 duration of all microstates was significantly increased during unresponsiveness ($P_{state, A} = 0.0001,$
382 $P_{state, B} = 0.003, P_{state, C} = 0.0001, P_{state, D} = 3e^{-6}$), in agreement with previous literature (Brodbeck et al.,
383 2012). Notably, microstate D had a striking increase in duration (Fig. 4A). At the same time, the
384 temporal coverage of class D was significantly higher during unresponsiveness (Fig. 4B), whereas the
385 coverage of microstate B was significantly lower during the same period ($P_{state, A} = 0.056, P_{state, B} =$
386 $0.001, P_{state, C} = 0.26, P_{state, D} = 1e^{-5}$). Similarly, the GEV of microstate D (Fig. 4C) was increased during
387 unresponsiveness, while the GEV of microstates A and B were decreased ($P_{state, A} = 0.0002, P_{state, B} =$
388 $0.0002, P_{state, C} = 0.17, P_{state, D} = 2e^{-5}$).

389 **Single-trial responsiveness prediction**

390 We verified whether microstate parameters in the pre-stimulus window are able to dissociate
391 responsiveness from unresponsiveness at an individual trial level during the full recordings, and
392 whether these properties could be generalised across subjects.

393 Out of all trials, 8% contained a button press event during the five seconds preceding each stimulus
394 and were excluded from further analysis. The remaining data had a balanced distribution of 1078
395 responses and 1117 misses out of a total of 2195 trials.

396 Training a radial basis function kernel support-vector machine repeatedly on the combined-
397 microstate and microstate-wise features to predict the binary outcome of a trial, as a response or a
398 miss, using one-subject-out cross-validation, confirmed that microstate dynamics were able to
399 predict responsiveness at an individual trial level and across subjects, with a performance similar to
400 that of the established theta-alpha ratio of spectral power (Fig. 5).

401 Combining the duration, temporal coverage, and GEV of each microstate to obtain a 4 x 5 input
402 feature vector for each trial achieved a mean AUC of 0.8552 (mean classification accuracy of 75.2%).
403 In comparison, the theta-alpha ratio achieved a mean AUC of 0.8519 (mean classification accuracy of
404 74.24%). A Wilcoxon signed rank test did not find significant differences between these performance
405 distributions. When combined, the microstate features and the theta-alpha ratio obtained a mean
406 AUC 0.8622 (mean classification accuracy of 77.1%).

407 When used individually as input features for the classification, mean microstate duration performed
408 remarkably well, achieving a mean AUC 0.8484 (mean classification accuracy of 76.1%). According to
409 Wilcoxon test, this was not significantly different from the classification performance of the
410 combined microstate parameters. The duration of microstate D was significantly better at predicting
411 responsiveness than microstates A-C ($p_{D-(A,B,C)} = \{0.0005, 0.0006, 0.002\}$).

412 It is worth noting that the one subject for whom the prediction performance was lower in the group
413 was Subject 12, who was also the only one whose alpha peak remained nearly unshifted after the
414 loss of responsiveness (Suppl. Fig. 2).

415 **Connectivity differences between microstates**

416 Having established the characteristic temporal patterns exhibited by microstate sequences before
417 and after drowsiness-induced loss of responsiveness, we next proceeded to investigate their
418 relationship with the underlying spectral content of the EEG, and the modulation of this relationship

419 as subjects become unresponsive. To this end, we investigated the power contributions and the
420 WPLI connectivity computed across samples belonging to each microstate before and after the loss
421 of responsiveness. While we do not assume a direct relation between neural sources of EEG
422 microstates and EEG spectral power and connectivity, our aim is to assess whether the neural
423 sources of microstates and sources of spectral measures covary at a fine temporal scale.

424 The spectral power contribution (Fig. 6A) displayed the characteristic alpha peak around 10 Hz
425 during the responsive period, which faded during the unresponsive period into high power at low
426 frequencies. This pattern was similar during all microstates.

427 Likewise, spectral connectivity (Fig. 6B) showed a peak at 10 Hz during responsiveness during all
428 microstates, which faded during unresponsiveness. The only pattern dissociating between
429 microstates during responsiveness was a decreased 10 Hz peak during microstate A. On the other
430 hand, there was a noticeable difference in the level of connectivity during unresponsiveness
431 between all microstate periods, with microstates D and A exhibiting the highest and the lowest
432 connectivity, respectively.

433 The effect size of the interaction between microstate and behavioural state (responsiveness and
434 unresponsiveness) computed individually at each frequency was indeed generally higher in
435 connectivity than in power (Fig. 6C). The effect size was largest in connectivity at 5.5 Hz and 10 Hz,
436 corresponding to the theta and alpha peaks displayed during all microstates during the unresponsive
437 and responsive periods, respectively. A peak in power contribution was also found at 13.5 Hz,
438 potentially due to the emergence of sleep spindles at the onset of sleep.

439 We also attempted to use pre-stimulus WPLI connectivity levels at alpha and theta frequencies in
440 order to train a classifier to predict responsiveness, using the same procedure as for the microstate
441 spatiotemporal parameters. No classifiers could be obtained that exceeded a 60% mean accuracy,
442 either microstate-wise or on the full set of pre-stimulus samples.

443 **Connectivity during microstate D after the loss of responsiveness**

444 Gathering from the evidence of increased temporal presence of microstate D after the loss of
445 responsiveness, as well as the higher connectivity displayed during this microstate during
446 unresponsiveness in comparison with the microstates A-C, we next sought to understand the
447 spectral connectivity patterns captured during microstate D in the selected alpha and theta ranges
448 during the unresponsiveness period.

449 Previous literature suggests that anterior (frontal) and posterior (parietal) scalp regions of interest
450 (ROI) show key changes in connectivity at the onset of sleep (Morikawa et al., 1997; Tanaka et al.,
451 2000, 1998; Wright et al., 1995), during sedation and after brain injury (Chennu et al. 2017; Chennu
452 et al. 2014; Chennu et al. 2016). Building upon this, we investigated the within-anterior, within-
453 posterior and between anterior-posterior connectivity during microstate D in comparison with
454 microstates A-C. For this purpose, we performed three repeated measures ANOVA tests to compare
455 the median connectivity during microstate D and that during each of the microstates A-C in each of
456 the six conditions (two frequency bands X three scalp ROIs) during the unresponsive period. Within
457 each condition, we corrected for the false discovery rate across the three tests (D vs A, D vs B and D
458 vs C) using Storey's procedure (Storey, 2002).

459 Fig. 7 exemplifies the most prominent differences we found in connectivity between samples
460 covered by microstate D and microstates A-C respectively, during unresponsiveness.

461 At the selected theta peak, the t-test results showed significantly higher median connectivity within
462 the anterior region during microstate D compared to each of the other microstates ($P_{D-\{A,B,C\}} = \{0.001,$
463 $0.008, 0.001\}$, $t_{D-\{A,B,C\}} = \{3.958, 3.069, 4.088\}$, Cohen's $d_{D-\{A,B,C\}} = \{0.990, 0.767, 1.022\}$). Median
464 connectivity between the anterior and posterior regions was also significantly higher during
465 microstate D than in microstates A and C ($P_{D-\{A,B,C\}} = \{0.003, 0.297, 0.003\}$, $t_{D-\{A,B,C\}} = \{3.578, 1.081,$
466 $3.392\}$, Cohen's $d_{D-\{A,B,C\}} = \{0.894, 0.27, 0.848\}$). No significant differences were found in median
467 connectivity within the posterior area.

468 Conversely, at the selected alpha peak, the repeated measures ANOVA showed significantly lower
469 median connectivity within the posterior area during microstate D compared to microstates A-C
470 ($P_{D-\{A,B,C\}} = \{0.033, 0.037, 0.033\}$, $t_{D-\{A,B,C\}} = \{2.686, 2.294, 2.559\}$, Cohen's $d_{D-\{A,B,C\}} = \{0.672, 0.573, 0.67\}$).

471 At the same time, microstate D captured significantly higher within-anterior median connectivity
472 than microstate A ($P_{D-\{A,B,C\}} = \{0.043, 0.617, 0.055\}$, $t_{D-\{A,B,C\}} = \{2.769, 0.511, 2.297\}$, Cohen's
473 $d_{D-\{A,B,C\}} = \{0.692, 0.128, 0.574\}$). No significant difference in median connectivity between anterior
474 and posterior regions was found during microstate D compared to microstates A-C.

475 These results confirmed that the timecourse of microstate D uniquely capture a simultaneous
476 disintegration of posterior alpha connectivity and emergence of frontal theta connectivity, which is
477 associated with the suppression of responsiveness at the onset of sleep.

478 Discussion

479 Summary

480 In this study, we used high-density EEG to explore the transient spatiotemporal and spectral
481 dynamics of electrical brain activity before and after the loss of behavioural responsiveness due to
482 drowsiness. Importantly, we examined the loss of responsiveness as participants became drowsy
483 while performing a discrimination task. Hence by design, our study is in contrast to and
484 complements studies of resting brain activity in the absence of any task, which have often focused
485 on an investigation of canonical sleep stages. Here, unresponsiveness – the failure to respond to the
486 auditory cues elicited by increased drowsiness – provided an objective and non-invasive behavioural
487 criterion in the transitional stage in between full wakefulness and early sleep.

488 To summarise our findings, we have shown that differences in spectral power and connectivity after
489 the loss of responsiveness that have been previously shown to differentiate between healthy
490 wakefulness and sleep, sedation and disorders of consciousness: a decrease in posterior alpha
491 power and the emergence of theta power, as well as the disintegration of frontoparietal connectivity
492 in alpha band. Further, microstate characteristics before and after the loss of responsiveness not
493 only correlate with behaviour at the group level, but also predict behaviour at the level of individual
494 experimental trials - when microstate D occurred more often during the pre-stimulus period,
495 participants were less likely to generate a response to the subsequent stimulus. This relationship
496 highlights a possible functional role of this microstate in modulating behaviour, and the predictive
497 power of this signature to define the capacity to consciously respond to abstract/semantic stimuli.
498 Finally, we discovered that while relative spectral power is similar across the temporal microstates,
499 spectral connectivity is more distinctive. This non-uniform pattern of connectivity across microstates
500 is modulated by the loss of responsiveness: the timecourse of microstate D captured significantly
501 increased connectivity in the theta band after the loss of responsiveness, underpinning a novel
502 profile of interaction between the temporal sequence of microstates and spectral brain connectivity.

503 Alpha power and connectivity characterise responsive wakefulness

504 Our analysis of EEG connectivity before microstate segmentation strengthens the evidence for the
505 fundamental role of the alpha networks in sustaining a state of responsive wakefulness. It is
506 important to clarify that attribution of connectivity to specific neuroanatomy is limited by the scalp-
507 level analysis we have conducted here, though previous research provides some pointers as to its
508 neural origins. An independent study by Chennu et al. (2017) involving a different group of healthy

509 adults and patients with brain injury has provided indirect information about the potential drivers of
1 resting alpha connectivity, by correlating it with resting metabolism measured with PET imaging. As
2 510 demonstrated in that study, the presence of a robust connectivity network in the alpha band was
3 511 correlated with metabolic activity in frontal and parietal cortices encompassing both intrinsic and
4 512 extrinsic awareness networks (Vanhaudenhuyse et al. 2010). Further, the body of literature based on
5 513 simultaneous EEG-fMRI recordings (Laufs et al. 2003a; Laufs et al. 2003b) has indicated negative
6 514 correlations between alpha power and BOLD activity of frontoparietal areas known to be part of the
7 515 attentional external awareness network. However, further research is needed to pinpoint the
8 516 cortical and subcortical sources of the connectivity patterns and changes we have elucidated here.
9 517
10 518 Our analysis of scalp-level connectivity highlights that it is not the full disappearance of all
11 519 connectivity that drives the loss of responsiveness, but specifically connectivity at alpha frequency.
12 520 Indeed, literature shows that connectivity shifts from alpha into lower-frequency theta and delta
13 521 frequencies in many contexts. This shift happens when consciousness fades (Chennu et al., 2016,
14 522 2014; Ogilvie, 2001; Tanaka et al., 2000, 1998; Wright et al., 1995), but also during natural
15 523 fluctuations in alpha power during resting wakefulness, which accompany increases in theta power
16 524 and BOLD activity in occipital and parietal areas (Laufs et al. 2006). In the larger picture of states and
17 525 levels of consciousness, our findings confirm long-range alpha networks as a common marker of
18 526 consciousness, whether this impairment is natural (sleep), pathological (disorders of consciousness)
19 527 or pharmacological (sedation).

528 **Microstate D predicts responsiveness across subjects**

529 Upon examining the spatiotemporal parameters of the canonical EEG microstates, we found an
38 530 increase in temporal coverage after the loss of responsiveness uniquely specific to microstate D,
39 531 along with an increase in its global explained variance, as compared to responsive periods. While the
40 532 duration of all microstates was longer during unresponsiveness, the duration of microstate D had a
41 533 prominent relative increase. In contrast, the temporal coverage of microstate B decreased in the
42 534 unresponsive period, as did the global explained variance of microstates A and B. Further, we
43 535 demonstrated that the general state of awareness, as reflected in the ongoing dynamics of pre-
44 536 stimulus EEG microstates, are indeed informative of the capacity of a subject to respond to a
45 537 stimulus during drowsiness at an individual trial level. This finding echoes similar evidence from the
46 538 literature, where pre-stimulus microstate properties predict perception of weak stimuli (Britz et al.
47 539 2014), accuracy of working memory (Muthukrishnan et al. 2016) and perceptual shifts between
48 540 bistable stimuli (Britz et al. 2009). Again, the special significance of microstate D during

1
2
3
4
5
6
7
8
9
10
11
12
13
14
15
16
17
18
19
20
21
22
23
24
25
26
27
28
29
30
31
32
33
34
35
36
37
38
39
40
41
42
43
44
45
46
47
48
49
50
51
52
53
54
55
56
57
58
59
60
61
62
63
64
65

541 unresponsiveness was visible from its increased ability to predict the likelihood of a response, in
542 comparison with microstates A-C. In addition, we showed that the increase in duration of this
543 microstate is the best predictor of responsiveness among all the microstate parameters.

544 We note that the durations of the microstates we obtained were significantly lower than previous
545 reports in the literature (Brodbeck et al. 2012; Tomescu et al. 2014; Tomescu et al. 2018). This might
546 be due in part to our analytical methodology: as specified in the methods, we used a smoothing
547 neighbourhood of 20ms, in keeping with the range of mean microstate durations reported in the re-
548 analysis of data from (Brodbeck et al. 2012) reported by Gärtner et al. (2015, Neuroimage).
549 However, our smaller durations could also be attributed to the fact that our participants were
550 performing an experimental task, which might have led to more rapid changes in dynamical brain
551 states. This was in contrast to the reports above, in which data were collected in the absence of any
552 task. Nevertheless, despite the shorter durations, we confirmed the expected presence of WPLI
553 connectivity in the alpha band within each microstate during wakefulness. Speculatively, the finer
554 temporal granularity of our microstate decomposition might have made the differences in
555 connectivity between microstates more apparent during the transition to sleep.

556 Our usage of machine learning allows us to quantify the performance of the model using its
557 discrimination accuracy, which speaks for the real-world applicability of the method (Breiman,
558 2001). Moreover, one-subject-out cross-validation allows us to infer that these results are
559 generalizable across people. At the same time, as expected, individual variability caps the maximum
560 possible accuracy when predicting responsiveness. Our results suggest that this cap is around an
561 accuracy of 75% (mean AUC around 0.85). Interestingly, the theta-alpha ratio, which we used as a
562 baseline given its sensitivity as a sleep index (Šušmáková and Krakovská, 2007), achieved a similar
563 classification accuracy as the microstate-based input features. This suggests that microstate
564 dynamics and spectral oscillations are potentially correlated. Intriguingly, we were not able to use
565 connectivity as a feature to train a suitable classifier for responsiveness during drowsiness, either
566 considering or ignoring the microstate sequence, despite strong evidence of major connectivity
567 changes occurring before and after the loss of responsiveness. This suggests that connectivity better
568 predicts the level of consciousness estimated over longer time scales, whereas spatiotemporal
569 microstate dynamics capture short-term changes in brain state that predict responsiveness.

570 **Microstate D captures a distinct connectivity profile after loss of responsiveness**

571 Alongside the distinctive increase in temporal coverage and duration of microstate D, we found a
572 singular spectral connectivity pattern during this microstate after loss of responsiveness, indicating

573 increased median connectivity in theta band, particularly in connections within frontal and between
574 frontal and parietal electrodes. At the same time, median posterior connectivity during microstate D
575 was reduced during unresponsiveness. Hence, the timecourse of microstate D appears to uniquely
576 capture a connectivity pattern specific to deeper stages of sleep, in comparison with other
577 microstates present during the same sleep stage. (Britz et al., 2010) correlated the microstate
578 timecourses with the timecourse of average spectral power within canonical frequency bands. They
579 reported finding no relationship between microstate dynamics and the spectral properties of the
580 EEG signal. Our findings represent the first demonstration that in fact, spectral brain connectivity in
581 fact presents a significant interaction with temporal microstate dynamics, underpinned by the
582 connectivity captured by microstate D. Estimation of connectivity from EEG can be affected by
583 volume conduction and referencing method. We have aimed to minimise the influence of the former
584 with the use of WPLI-based connectivity. Further, we verified that re-analysis of WPLI connectivity
585 with reference-free current source density estimates (Kayser and Tenke 2015) identified strong
586 interactions in the alpha and theta bands, similar to those presented in Fig. 6B (see Suppl. Fig. 5).

587 There currently exists no consensus on the meaning of individual microstates in terms of their neural
588 generators. However, microstate D has occasionally been linked to attentional networks. In a study
589 of fMRI resting-state networks, (Britz et al., 2010) showed a higher correlation of microstate D with
590 ventral and dorsal frontoparietal networks, functionally associated with attention switching and
591 directing attention towards external salient stimuli. A decreased duration of this microstate has
592 been reported in schizophrenia (Koenig et al., 1999; Lehmann et al., 2005; Nishida et al., 2013;
593 Tomescu et al., 2014) and hallucination (Kindler et al., 2011) – two conditions involving impairments
594 in task switching and attention (Collerton et al., 2005; Cornblatt and Keilp, 1994). An investigation of
595 modalities of thinking found an increased microstate D duration in resting-state compared to visual
596 and verbal task periods (Milz et al., 2015); this was also interpreted as a confirmation of the
597 previously-mentioned study by (Britz et al., 2010) due to a higher probability of attention switching
598 during rest (high microstate D duration), as opposed to performing a single goal-oriented task (lower
599 microstate D duration). On the other hand, (Seitzman et al., 2016) have found an increased duration
600 of microstate D during a cognitive task as compared to wakeful rest.

601 Given the weak evidence in the literature associating microstate D with task-related attention
602 networks, we are cautious in interpreting our findings on this basis. A previous study on the same
603 data (Kouider et al., 2014) found that a correct response to stimuli is still prepared during
604 unresponsiveness, suggesting preserved attention. It is possible that our findings indicate more
605 demand from attention networks as drowsiness increases and subjects become unable to respond to

606 the task. In study of microstates during sleep in the absence of any task, (Brodbeck et al., 2012) did
607 not observe an increase in this microstate during sleep. This suggests that microstate D might indeed
608 be specifically related to the experimental task. Further, this interpretation is compatible with a
609 study by Katayama et al. (Katayama et al., 2007), which found that the duration of microstate D was
610 increased in light (but not deep) hypnosis, a state which produces similar EEG patterns to sleep-
611 induced unresponsiveness (Barker and Burgwin, 1949).

612 Nonetheless, the spatiotemporal and spectral connectivity dynamics observed in microstate D after
613 the loss of responsiveness yield an important insight into the dynamics of the transition to sleep.
614 While connectivity averaged during all microstates reflects typical changes commonly found in the
615 loss of consciousness in the onset of sleep, anaesthesia or disorders of consciousness – weaker alpha
616 and stronger theta long-range networks – the individual timecourse of microstate D captures
617 significantly stronger patterns, despite having a duration no longer than 40ms. This suggests that,
618 after the loss of responsiveness, the process of falling asleep is not necessarily linear, but rather
619 consists of an interplay between distinct networks, captured by different microstates, which are at
620 different points along the transition between wakeful and asleep modes of operation. It is worth
621 noting that many subjects often became variable in their response times, and eventually
622 unresponsive, within 5-7 minutes of starting the recording (see Fig. 1), highlighting the natural onset
623 of drowsiness that could confound many experimental designs, if not appropriately controlled for
624 (Noreika et al. 2017; Tagliazucchi and Laufs 2014). Further, our work might lend itself to explaining
625 one of the current riddles of sleep research: why is it that, despite the establishment of a series of
626 clear EEG markers delimiting wake and several stages of sleep, finding an EEG-based threshold to
627 separate between the subjective intuition of being awake or asleep has not yet been achieved?
628 Indeed, it has been reported by Hori et al. (1994) that 26% of all subjects stated that they had been
629 awake at times when their EEG was classified as stage 2 sleep, which is commonly used to define
630 “true sleep” (Ogilvie, 2001). The rapid fluctuation of brain networks, some of which are closer to
631 wakefulness (during microstates A-C) and others closer to sleep (during microstate D) could be the
632 reason why our momentary introspective state of being “awake” and “asleep” might not concur with
633 a coarse-grained assessment of EEG over many seconds of data, as usually done during the
634 identification of sleep stages. Instead, our findings here highlight that further research should focus
635 on the rapidly changing dynamics of brain networks that appear to capture key dynamics relevant to
636 our behavioural and perhaps even introspective state, as we drift into unconsciousness.

637 Acknowledgements

638 We thank Louise Goupil for collecting the data for this experiment.

639 Figure Legends

640 **Figure 1. Reaction times and data segmentation into responsiveness and unresponsiveness for individual**
641 **participants.** The horizontal axis represents recording time and the vertical axis represents reaction time in
642 seconds. Blue markers indicate responses, while orange markers indicate misses. The blue area corresponds to
643 the five-minute period of responsiveness, while the orange area corresponds to the five-minute period of
644 unresponsiveness.

645 **Figure 2. Spectral power topography and WPLI frontoparietal connectivity at alpha (9.5-10.5 Hz) and theta**
646 **(5-6 Hz) peaks before and after the loss of responsiveness.** Values are averaged across participants. With loss
647 of responsiveness, power over parietal sensors and connectivity between frontal and parietal sensors shifted
648 from the alpha to the theta band.

649 **Figure 3. Microstate topographies computed across all subjects.** These topographies are plotted in
650 correspondence with the four canonical microstate topographies commonly described in literature.
651 Microstate topographies reported by Brodbeck et al. (2012) and Koenig et al. (2002) are shown for
652 comparison (reproduced here with permission).

653 **Figure 4. Microstate parameters before and after the loss of responsiveness in drowsiness.** Within each
654 panel of grouped scatter box plots, inner boxes represent the standard error of the mean for each microstate
655 parameter, and outer boxes represent the standard deviation. The mean is shown by a continuous line, the
656 median is shown by a dotted line, and individual participants are shown as dots. Asterisks show a significant
657 within-subject main effect of state for a microstate. Duration, temporal coverage and GEV of microstate D all
658 significantly increased during unresponsiveness.

659 **Figure 5. Classification performance, computed as the area under the ROC curve, for a support-vector**
660 **machine (SVM) trained using 5 seconds of pre-stimulus data to classify responses and misses.** Input features
661 to the classifier were microstate parameters or the theta-alpha ratio, individually or combined. Within each
662 group of grouped scatter box plots, inner boxes represent the standard error of the mean, outer boxes
663 represent the standard deviation. The mean is shown by a yellow line, the median is shown by a green line
664 (where distinct from the mean), and individual participants are shown as dots. Microstate parameters were
665 able to predict responsiveness at an individual trial level across subjects, with a performance similar to that of
666 the theta-alpha ratio.

667 **Figure 6. Spectral power (panel A) and WPLI connectivity (panel B) captured during individual microstates**
668 **before and after loss of responsiveness due to drowsiness.** Channel-wise relative power at each frequency
669 bin was calculated as the power at that bin as a percentage of total power within 1-20Hz. Within each subject,
24

670 for both relative power and WPLI connectivity, the median across channels is plotted. Figures show the grand
671 average over all subjects. Panel C shows the effect size, computed as Cohen's *d*, of the interaction between
672 behavioural state and microstate at each frequency bin for power contributions and for connectivity. By
673 convention, 0.2, 0.5 and 0.8 denote small, medium and large effect sizes, respectively. The interaction
674 between microstate and behavioural state was stronger in connectivity than in power.

675 **Figure 7. Frontal and frontoparietal WPLI connectivity at theta peak (5-6 Hz).** Microstate D captured
676 significantly higher theta connectivity within frontal and between frontoparietal sensors during
677 unresponsiveness, compared to microstates A-C.

678 References

- 679 Alkire, M.T., Hudetz, A.G., Tononi, G., 2008. Consciousness and Anesthesia. *Science* (80-.). 322, 876–880.
- 680 Badia, P., Wright, K.P.J., Wauquier, A., 1994. Fluctuations in single-hertz EEG activity during the transition to
681 sleep. *Sleep onset Norm. Abnorm. Process.* 201–218.
- 682 Baker, A.P., Brookes, M.J., Rezek, I. a., Smith, S.M., Behrens, T., Smith, P.J.P., Woolrich, M., 2014. Fast transient
683 networks in spontaneous human brain activity. *Elife* 2014, 1–18.
- 684 Bareham, C. a, Manly, T., Pustovaya, O. V, Scott, S.K., Bekinschtein, T. a, 2014. Losing the left side of the world:
685 rightward shift in human spatial attention with sleep onset. *Sci. Rep.* 4, 5092.
- 686 Barker, W., Burgwin, S., 1949. Brain wave patterns during hypnosis, hypnotic sleep and normal sleep. *Arch.*
687 *Neurol. Psychiatry* 62, 412–20.
- 688 Barry, R.J., Clarke, A.R., Johnstone, S.J., Magee, C.A., Rushby, J.A., 2007. EEG differences between eyes-closed
689 and eyes-open resting conditions. *Clin. Neurophysiol.* 118, 2765–73.
- 690 Bell, A., Sejnowski, T.J., 1995. Fast blind separation based on information theory. *Proc. Intern. Symp. Nonlinear*
691 *Theory ...* 1, 43–47.
- 692 Block, N., 1996. How can we find the neural correlate of consciousness? *Trends Neurosci.* 19, 456–9.
- 693 Britz, J., Van De Ville, D., Michel, C.M., 2010. BOLD correlates of EEG topography reveal rapid resting-state
694 network dynamics. *Neuroimage* 52, 1162–1170.
- 695 Brodbeck, V., Kuhn, A., von Wegner, F., Morzelewski, A., Tagliazucchi, E., Borisov, S., Michel, C.M., Laufs, H.,
696 2012. EEG microstates of wakefulness and NREM sleep. *Neuroimage* 62, 2129–2139.
- 697 Broughton, R., Hasan, J., 1995. Quantitative topographic electroencephalographic mapping during drowsiness
698 and sleep onset. *J. Clin. Neurophysiol.* 12, 372–386.
- 699 Cantero, J.L., Atienza, M., Salas, R.M., Gómez, C.M., 1999. Brain spatial microstates of human spontaneous

- 700 alpha activity in relaxed wakefulness, drowsiness period, and REM sleep. *Brain Topogr.* 11, 257–263.
- 701 Chennu, S., Finoia, P., Kamau, E., Allanson, J., Williams, G.B., Monti, M.M., Noreika, V., Arnatkeviciute, A.,
702 Canales-Johnson, A., Olivares, F., Cabezas-Soto, D., Menon, D.K., Pickard, J.D., Owen, A.M., Bekinschtein,
703 T. a., 2014. Spectral Signatures of Reorganised Brain Networks in Disorders of Consciousness. *PLoS*
704 *Comput. Biol.* 10, e1003887.
- 705 Chennu, S., O'Connor, S., Adapa, R., Menon, D.K., Bekinschtein, T.A., 2016. Brain Connectivity Dissociates
706 Responsiveness from Drug Exposure during Propofol-Induced Transitions of Consciousness. *PLOS*
707 *Comput. Biol.* 12, e1004669.
- 708 Christianini, N., Shawe-Taylor, J., 2000. Support vector machines. Cambridge University Press, Cambridge, UK.
- 709 Collerton, D., Perry, E., McKeith, I., 2005. Why people see things that are not there: a novel Perception and
710 Attention Deficit model for recurrent complex visual hallucinations. *Behav. Brain Sci.* 28, 737-57-94.
- 711 Cornblatt, B.A., Keilp, J.G., 1994. Impaired attention, genetics, and the pathophysiology of schizophrenia.
712 *Schizophr. Bull.* 20, 31–46.
- 713 Davis, J., Goadrich, M., 2006. The Relationship Between Precision-Recall and ROC Curves. *Proc. 23rd Int. Conf.*
714 *Mach. Learn. -- ICML'06* 233–240.
- 715 De Gennaro, L., Ferrara, M., Curcio, G., Cristiani, R., 2016. Antero-posterior EEG changes during the
716 wakefulness and sleep transition. *Clin. Neurophysiol.* 112, 1901–1911.
- 717 Delorme, A., Makeig, S., 2004. EEGLAB: An open source toolbox for analysis of single-trial EEG dynamics
718 including independent component analysis. *J. Neurosci. Methods* 134, 9–21.
- 719 Farooqui, A.A., Manly, T., 2017. When Attended and Conscious Perception Deactivates Fronto-Parietal
720 Regions. *Cortex* 1–14.
- 721 Gärtner, M., Brodbeck, V., Laufs, H., Schneider, G., 2015. A stochastic model for EEG microstate sequence
722 analysis. *Neuroimage* 104, 199–208.
- 723 Giacino, J.T., Fins, J.J., Laureys, S., Schiff, N.D., 2014. Disorders of consciousness after acquired brain injury: the
724 state of the science. *Nat. Rev. Neurol.* 10, 99–114.
- 725 Gibbons, J.D., Chakraborti, S., 2011. Nonparametric statistical inference. Springer.
- 726 Goupil, L., Bekinschtein, T. a., 2012. Cognitive processing during the transition to sleep. *Arch. Ital. Biol.* 150,
727 140–154.
- 728 Greenhouse, S.W., Geisser, S., 1959. On methods in the analysis of profile data. *Psychometrika* 24, 95–112.
- 729 Grieder, M., Koenig, T., Kinoshita, T., Utsunomiya, K., Wahlund, L.O., Dierks, T., Nishida, K., 2016. Discovering

- 730 EEG resting state alterations of semantic dementia. *Clin. Neurophysiol.* 127, 2175–2181.
- 1
2 731 Hobson, J.A., Pace-Schott, E.F., 2002. The cognitive neuroscience of sleep: neuronal systems, consciousness
3 and learning. *Nat. Rev. Neurosci.* 3, 679–93.
- 4 732
5
6 733 Hogg, R. V., Ledolter, J., 1987. *Engineering Statistics*. MacMillan, New York.
- 7
8 734 Hori, T., Hayashi, M., Morikawa, T., 1994. Topographical EEG changes and the hypnagogic experience., in:
9 Sleep Onset: Normal and Abnormal Processes. American Psychological Association, Washington, pp.
10 735 237–253.
- 11 736
12
13 737 Iber, C., Ancoli-Israel, S., Chesson Jr., A.L., Quan, S.F., 2007. *The AASM Manual for the Scoring of Sleep and*
14 *Associated Events: Rules Terminology and Technical Specifications* 1st ed.
- 15 738
16
17 739 Katayama, H., Gianotti, L.R.R., Isotani, T., Faber, P.L., Sasada, K., Kinoshita, T., Lehmann, D., 2007. Classes of
18 740 multichannel EEG microstates in light and deep hypnotic conditions. *Brain Topogr.* 20, 7–14.
- 19
20
21 741 Khanna, A., Pascual-Leone, A., Farzan, F., 2014. Reliability of Resting-State Microstate Features in
22 742 Electroencephalography. *PLoS One* 9, e114163.
- 23
24
25 743 Kikuchi, M., Koenig, T., Munesue, T., Hanaoka, A., Strik, W., Dierks, T., Koshino, Y., Minabe, Y., 2011. EEG
26 744 microstate analysis in Drug-Naive patients with panic disorder. *PLoS One* 6, 2–7.
- 27
28
29 745 Kikuchi, M., Koenig, T., Wada, Y., Higashima, M., Koshino, Y., Strik, W., Dierks, T., 2007. Native EEG and
30 746 treatment effects in neuroleptic-naïve schizophrenic patients: Time and frequency domain approaches.
31 *Schizophr. Res.* 97, 163–172.
- 32 747
33
34 748 Kindler, J., Hubl, D., Strik, W.K., Dierks, T., Koenig, T., 2011. Resting-state EEG in schizophrenia: Auditory verbal
35 749 hallucinations are related to shortening of specific microstates. *Clin. Neurophysiol.* 122, 1179–1182.
- 36
37
38 750 Koch, C., Massimini, M., Boly, M., Tononi, G., 2016. Neural correlates of consciousness: progress and problems.
39 751 *Nat. Rev. Neurosci.* 17, 307–321.
- 40
41
42 752 Koenig, T., Brandeis, D., 2016. Inappropriate assumptions about EEG state changes and their impact on the
43 753 quantification of EEG state dynamics. *Neuroimage* 125, 1104–1106.
- 44
45
46 754 Koenig, T., Lehmann, D., Merlo, M.C.G., Kochi, K., Hell, D., Koukkou, M., 1999. A deviant EEG brain microstate
47 755 in acute, neuroleptic-naïve schizophrenics at rest. *Eur. Arch. Psychiatry Clin. Neurosci.* 249, 205–211.
- 48
49
50 756 Koenig, T., Prichep, L., Lehmann, D., Sosa, P.V., Braeker, E., Kleinlogel, H., Isenhardt, R., John, E.R., 2002.
51 757 Millisecond by millisecond, year by year: normative EEG microstates and developmental stages.
52 758 *Neuroimage* 16, 41–48.
- 53
54
55 759 Koenig, T., Studer, D., Hubl, D., Melie, L., Strik, W.K., 2005. Brain connectivity at different time-scales measured
56 760 with EEG. *Philos. Trans. R. Soc. B Biol. Sci.* 360, 1015–1024.
- 57
58
59
60
61
62
63
64
65

- 1 761 Kouider, S., Andrillon, T., Barbosa, L.S., Goupil, L., Bekinschtein, T.A., 2014. Inducing Task-Relevant Responses
2 762 to Speech in the Sleeping Brain. *Curr. Biol.* 24, 2208–2214.
- 3
4 763 Kuhn, A., Brodbeck, V., Tagliazucchi, E., Morzelewski, A., von Wegner, F., Laufs, H., 2015. Narcoleptic Patients
5 764 Show Fragmented EEG-Microstructure During Early NREM Sleep. *Brain Topogr.* 28, 619–635.
- 6
7 765 Laureys, S., 2005. The neural correlate of (un)awareness: lessons from the vegetative state. *Trends Cogn. Sci.*
8 766 9, 556–559.
- 9
10
11 767 Lechinger, J., Bothe, K., Pichler, G., Michitsch, G., Donis, J., Klimesch, W., Schabus, M., 2013. CRS-R score in
12 768 disorders of consciousness is strongly related to spectral EEG at rest. *J. Neurol.* 260, 2348–2356.
- 13
14
15 769 Lee, H., Mashour, G. a, Noh, G.-J., Kim, S., Lee, U., 2013. Reconfiguration of network hub structure after
16 770 propofol-induced unconsciousness. *Anesthesiology* 119, 1347–59.
- 17
18
19 771 Lehmann, D., 1990. Brain electric microstates and cognition: the atoms of thought, in: *Machinery of the Mind*.
20 772 Springer, pp. 209–224.
- 21
22
23 773 Lehmann, D., 1971. Multichannel topography of human alpha EEG fields. *Electroencephalogr. Clin.*
24 774 *Neurophysiol.* 31, 439–449.
- 25
26
27 775 Lehmann, D., Faber, P.L., Galderisi, S., Herrmann, W.M., Kinoshita, T., Koukkou, M., Mucci, A., Pascual-Marqui,
28 776 R.D., Saito, N., Wackermann, J., Winterer, G., Koenig, T., 2005. EEG microstate duration and syntax in
29 777 acute, medication-naïve, first-episode schizophrenia: A multi-center study. *Psychiatry Res.* -
30 778 *Neuroimaging* 138, 141–156.
- 31
32
33
34 779 Lehmann, D., Ozaki, H., Pal, I., 1987. EEG alpha map series: brain micro-states by space-oriented adaptive
35 780 segmentation. *Electroencephalogr. Clin. Neurophysiol.* 67, 271–288.
- 36
37
38 781 Lehmann, D., Pascual-Marqui, R.D., Strik, W.K., Koenig, T., 2010. Core networks for visual-concrete and
39 782 abstract thought content: A brain electric microstate analysis. *Neuroimage* 49, 1073–1079.
- 40
41
42 783 Lehmann, D., Skrandies, W., 1980. Reference-free identification of components of checkerboard-evoked
43 784 multichannel potential fields. *Electroencephalogr. Clin. Neurophysiol.* 48, 609–621.
- 44
45
46 785 Marple, L., 1999. Computing the discrete-time “analytic” signal via FFT. *IEEE Trans. Signal Process.* 47, 2600–
47 786 2603.
- 48
49
50 787 Mauchly, J.W., 1940. Significance Test for Sphericity of a Normal n-Variate Distribution. *Ann. Math. Stat.* 11,
51 788 204–209.
- 52
53
54 789 Michel, C.M., Koenig, T., Brandeis, D., 2009. Electrical neuroimaging in the time domain, in: Michel, C.M.,
55 790 Koenig, T., Brandeis, D., Gianotti, L.R.R., Wackermann, J. (Eds.), *Electrical Neuroimaging*. Cambridge
56 791 University Press, Cambridge, pp. 111–144.

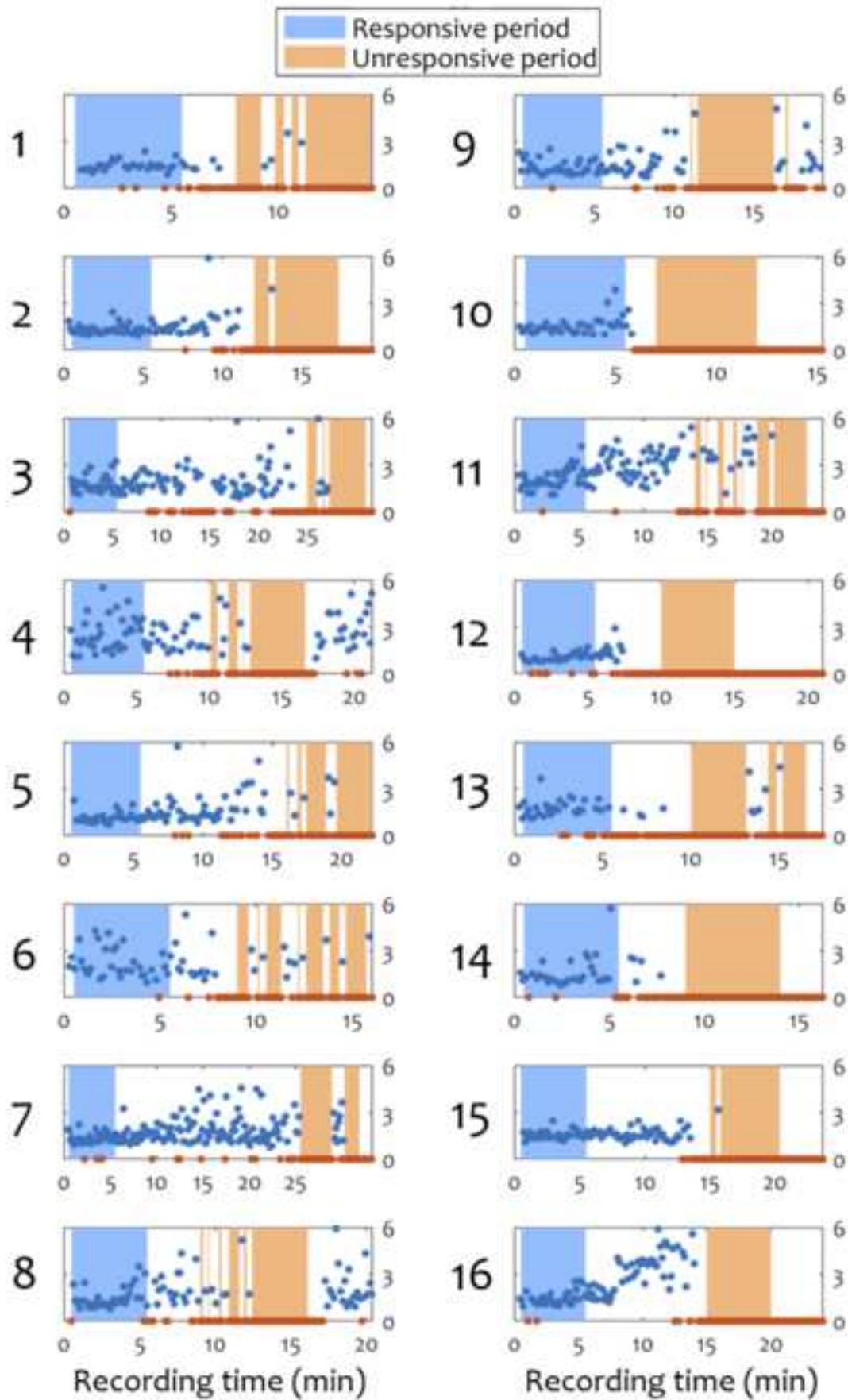
- 792 Milz, P., Faber, P.L., Lehmann, D., Koenig, T., Kochi, K., Pascual-Marqui, R.D., 2015. The functional significance
1 793 of EEG microstates—Associations with modalities of thinking. *Neuroimage* 125, 643–656.
2
3
4 794 Milz, P., Pascual-Marqui, R.D., Achermann, P., Kochi, K., Faber, P.L., 2017. The EEG microstate topography is
5 795 predominantly determined by intracortical sources in the alpha band. *Neuroimage* 162, 353–361.
6
7 796 Morikawa, T., Hayashi, M., Hori, T., 1997. Auto power and coherence analysis of delta-theta band EEG during
8 797 the waking-sleeping transition period. *Electroencephalogr. Clin. Neurophysiol.* 103, 633–641.
9
10 798 Murray, M.M., Brunet, D., Michel, C.M., 2008. Topographic ERP analyses: A step-by-step tutorial review. *Brain*
11 799 *Topogr.* 20, 249–264.
12
13 800 Niedermeyer, E., 2005a. The Normal EEG of the Waking Adult, in: Niedermeyer, E., Lopes Da Silva, F. (Eds.),
14 801 *Electroencephalography: Basic Principles, Clinical Applications, and Related Fields*. Lippincott Williams &
15 802 Wilkins, Philadelphia.
16
17 803 Niedermeyer, E., 2005b. Sleep and EEG, in: *Electroencephalography: Basic Principles, Clinical Applications, and*
18 804 *Related Fields*. Lippincott Williams & Wilkins, Philadelphia.
19
20 805 Nishida, K., Morishima, Y., Yoshimura, M., Isotani, T., Irisawa, S., Jann, K., Dierks, T., Strik, W., Kinoshita, T.,
21 806 Koenig, T., 2013. EEG microstates associated with salience and frontoparietal networks in
22 807 frontotemporal dementia, schizophrenia and Alzheimer’s disease. *Clin. Neurophysiol.* 124, 1106–1114.
23
24 808 Ogilvie, R.D., 2001. The process of falling asleep. *Sleep Med. Rev.* 5, 247–270.
25
26 809 Ogilvie, R.D., Wilkinson, R.T., 1984. The detection of sleep onset: behavioral and physiological convergence.
27 810 *Psychophysiology* 21, 510–520.
28
29 811 Overgaard, M., Overgaard, R., 2011. Measurements of consciousness in the vegetative state. *Lancet* 378,
30 812 2052–4.
31
32 813 Pascual-Marqui, R.D., Lehmann, D., Faber, P., Milz, P., Kochi, K., Yoshimura, M., Nishida, K., Isotani, T.,
33 814 Kinoshita, T., 2014. The resting microstate networks (RMN): cortical distributions, dynamics, and
34 815 frequency specific information flow. *arXiv Prepr. arXiv1411.1949* 1–14.
35
36 816 Pasqual-Marqui, R.D., Michel, C.M., Lehmann, D., 1995. Segmentation of brain electrical activity into
37 817 microstates: model estimation and validation. *IEEE Trans. Biomed. Eng.* 42, 658–665.
38
39 818 Platt, J.C., 1999. Probabilistic Outputs for Support Vector Machines and Comparisons to Regular Likelihood
40 819 Methods. *Adv. Large Margin Classif.*
41
42 820 Prerau, M.J., Hartnack, K.E., Obregon-Henao, G., Sampson, A., Merlino, M., Gannon, K., Bianchi, M.T.,
43 821 Ellenbogen, J.M., Purdon, P.L., 2014. Tracking the Sleep Onset Process: An Empirical Model of Behavioral
44 822 and Physiological Dynamics. *PLoS Comput. Biol.* 10, e1003866.
45
46
47
48
49
50
51
52
53
54
55
56
57
58

- 823 Purdon, P.L., Pierce, E.T., Mukamel, E. a, Prerau, M.J., Walsh, J.L., Wong, K.F.K., Salazar-Gomez, A.F., Harrell,
1 824 P.G., Sampson, A.L., Cimenser, A., Ching, S., Kopell, N.J., Tavares-Stoeckel, C., Habeeb, K., Merhar, R.,
2
3 825 Brown, E.N., 2013. Electroencephalogram signatures of loss and recovery of consciousness from
4
5 826 propofol. *Proc. Natl. Acad. Sci. U. S. A.* 110, E1142-51.
6
7 827 Sanders, R.D., Tononi, G., Laureys, S., Sleigh, J., 2013. Unconsciousness, not equal to unresponsiveness.
8
9 828 *Anesthesiology* 116, 946–959.
10
11 829 Schlegel, F., Lehmann, D., Faber, P.L., Milz, P., Gianotti, L.R.R., 2012. EEG Microstates During Resting Represent
12
13 830 Personality Differences. *Brain Topogr.* 25, 20–26.
14
15 831 Seitzman, B.A., Abell, M., Bartley, S.C., Erickson, M.A., Bolbecker, A.R., Hetrick, W.P., 2016. Cognitive
16
17 832 manipulation of brain electric microstates. *Neuroimage* 146, 0–1.
18
19 833 Steriade, M., McCormick, D., Sejnowski, T., 1993. Thalamocortical oscillations in the sleeping and aroused
20
21 834 brain. *Science* (80-). 262, 679–685.
22
23 835 Storey, J.D., 2002. A direct approach approach to false discovery rates. *J. R. Stat. Soc.* 64, 479–498.
24
25 836 Strelets, V., Faber, P.L., Golikova, J., Novototsky-Vlasov, V., Koenig, T., Gianotti, L.R.R., Gruzelier, J.H., Lehmann,
26
27 837 D., 2003. Chronic schizophrenics with positive symptomatology have shortened EEG microstate
28
29 838 durations. *Clin. Neurophysiol.* 114, 2043–2051.
30
31 839 Šušmáková, K., Krakovská, a, 2007. Classification of waking, sleep onset and deep sleep by single measures.
32
33 840 *Meas. Sci. Rev.* 7, 34–38.
34
35 841 Tanaka, H., Hayashi, M., Hori, T., 2000. Topographical characteristics of slow wave activities during the
36
37 842 transition from wakefulness to sleep. *Clin. Neurophysiol.* 111, 417–427.
38
39 843 Tanaka, H., Hayashi, M., Hori, T., 1998. Topographic mapping of electroencephalography coherence in
40
41 844 hypnagogic state. *Psychiatry Clin. Neurosci.* 52, 147–148.
42
43 845 Tanaka, H., Hayashi, M., Hori, T., 1997. Topographical characteristics and principal component structure of the
44
45 846 hypnagogic EEG. *Sleep* 20, 523–534.
46
47 847 Tomescu, M.I., Rihs, T. a., Becker, R., Britz, J., Custo, A., Grouiller, F., Schneider, M., Debbané, M., Eliez, S.,
48
49 848 Michel, C.M., 2014. Deviant dynamics of EEG resting state pattern in 22q11.2 deletion syndrome
50
51 849 adolescents: A vulnerability marker of schizophrenia? *Schizophr. Res.* 157, 175–181.
52
53 850 Tukey, J.W., 1949. Comparing individual means in the analysis of variance. *Biometrics* 5, 99–114.
54
55 851 Van de Ville, D., Britz, J., Michel, C.M., 2010. EEG microstate sequences in healthy humans at rest reveal scale-
56
57 852 free dynamics. *Proc. Natl. Acad. Sci. U. S. A.* 107, 18179–18184.
58
59 853 Vanhauzenhuysse, A., Demertzi, A., Schabus, M., Noirhomme, Q., Bredart, S., Boly, M., Phillips, C., Soddu, A.,
60
61
62
63
64
65

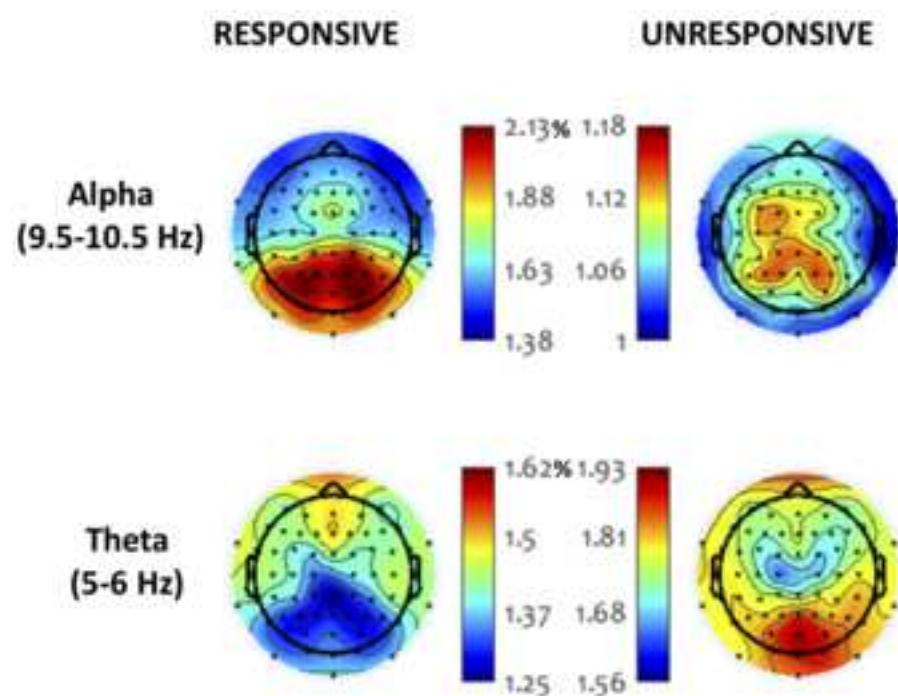
- 854 Luxen, A., Moonen, G., Laureys, S., 2011. Two Distinct Neuronal Networks Mediate the Awareness of
1 855 Environment and of Self. *J. Cogn. Neurosci.* 23, 570–578.
2
3
4 856 Vert, J., Tsuda, K., Schölkopf, B., 2004. A primer on kernel methods. *Kernel Methods Comput. Biol.* 35–70.
5
6 857 Vidaurre, D., Quinn, A.J., Baker, A.P., Dupret, D., Tejero-Cantero, A., Woolrich, M.W., 2016. Spectrally resolved
7 858 fast transient brain states in electrophysiological data. *Neuroimage* 126, 81–95.
8
9
10 859 Vinck, M., Oostenveld, R., van Wingerden, M., Battaglia, F., Pennartz, C.M.A., 2011. An improved index of
11 860 phase-synchronization for electrophysiological data in the presence of volume-conduction, noise and
12 861 sample-size bias. *Neuroimage* 55, 1548–65.
13
14
15 862 Wright, K.P., Badia, P., Wauquier, A., 1995. Topographical and temporal patterns of brain activity during the
16 863 transition from wakefulness to sleep. *Sleep* 18, 880–889.
17
18
19 864 Britz J, Diaz Hernandez L, Ro T, Michel CM (2014) EEG-microstate dependent emergence of perceptual
20 865 awareness *Front Behav Neurosci* 8:163 doi:10.3389/fnbeh.2014.00163
21
22
23 866 Britz J, Landis T, Michel CM (2009) Right parietal brain activity precedes perceptual alternation of bistable
24 867 stimuli *Cereb Cortex* 19:55-65 doi:10.1093/cercor/bhn056
25
26
27
28 868 Brodbeck V et al. (2012) EEG microstates of wakefulness and NREM sleep *Neuroimage* 62:2129-2139
29 869 doi:10.1016/j.neuroimage.2012.05.060
30
31
32 870 Chennu S et al. (2017) Brain networks predict metabolism, diagnosis and prognosis at the bedside in disorders
33 871 of consciousness *Brain* 140:2120-2132 doi:10.1093/brain/awx163
34
35
36
37 872 Chennu S et al. (2014) Spectral signatures of reorganised brain networks in disorders of consciousness *PLOS*
38 873 *Computational Biology* 10:e1003887 doi:10.1371/journal.pcbi.1003887
39
40
41 874 Chennu S, O'Connor S, Adapa R, Menon DK, Bekinschtein TA (2016) Brain Connectivity Dissociates
42 875 Responsiveness from Drug Exposure during Propofol-Induced Transitions of Consciousness *PLOS*
43 876 *Computational Biology* 12:e1004669 doi:10.1371/journal.pcbi.1004669
44
45
46
47 877 Kayser J, Tenke CE (2015) On the benefits of using surface Laplacian (current source density) methodology in
48 878 electrophysiology *International Journal of Psychophysiology* 97:171-173
49 879 doi:10.1016/j.ijpsycho.2015.06.001
50
51
52
53 880 Koenig T et al. (2002) Millisecond by millisecond, year by year: normative EEG microstates and developmental
54 881 stages *Neuroimage* 16:41-48 doi:10.1006/nimg.2002.1070
55
56
57 882 Laufs H, Holt JL, Elfont R, Krams M, Paul JS, Krakow K, Kleinschmidt A (2006) Where the BOLD signal goes when
58 883 alpha EEG leaves *NeuroImage* 31:1408-1418
59

1 884 Laufs H, Kleinschmidt A, Beyerle A, Eger E, Salek-Haddadi A, Preibisch C, Krakow K (2003a) EEG-correlated fMRI
2 885 of human alpha activity *NeuroImage* 19:1463-1476
3
4 886 Laufs H, Krakow K, Sterzer P, Eger E, Beyerle A, Salek-Haddadi A, Kleinschmidt A (2003b)
5
6 887 Electroencephalographic signatures of attentional and cognitive default modes in spontaneous brain
7
8 888 activity fluctuations at rest *Proc Natl Acad Sci U S A* 100:11053-11058 doi:10.1073/pnas.1831638100
9
10 889 Muthukrishnan SP, Ahuja N, Mehta N, Sharma R (2016) Functional brain microstate predicts the outcome in a
11
12 890 visuospatial working memory task *Behav Brain Res* 314:134-142 doi:10.1016/j.bbr.2016.08.020
13
14 891 Noreika V, Kamke MR, Canales-Johnson A, Chennu S, Mattingley JB, Bekinschtein TA (2017) Neurobehavioral
15
16 892 dynamics of drowsiness *bioRxiv* doi:10.1101/155754
17
18 893 Tagliazucchi E, Laufs H (2014) Decoding wakefulness levels from typical fMRI resting-state data reveals reliable
19
20 894 drifts between wakefulness and sleep *Neuron* 82:695-708 doi:10.1016/j.neuron.2014.03.020
21
22
23 895 Tomescu MI et al. (2014) Deviant dynamics of EEG resting state pattern in 22q11.2 deletion syndrome
24
25 896 adolescents: A vulnerability marker of schizophrenia? *Schizophr Res* 157:175-181
26
27 897 doi:10.1016/j.schres.2014.05.036
28
29 898 Tomescu MI et al. (2018) From swing to cane: Sex differences of EEG resting-state temporal patterns during
30
31 899 maturation and aging *Dev Cogn Neurosci* 31:58-66 doi:10.1016/j.dcn.2018.04.011
32
33 900 Vanhaudenhuyse A et al. (2010) Two Distinct Neuronal Networks Mediate the Awareness of Environment and
34
35 901 of Self *J Cog Neurosci* 23:570-578 doi:10.1162/jocn.2010.21488
36
37 902

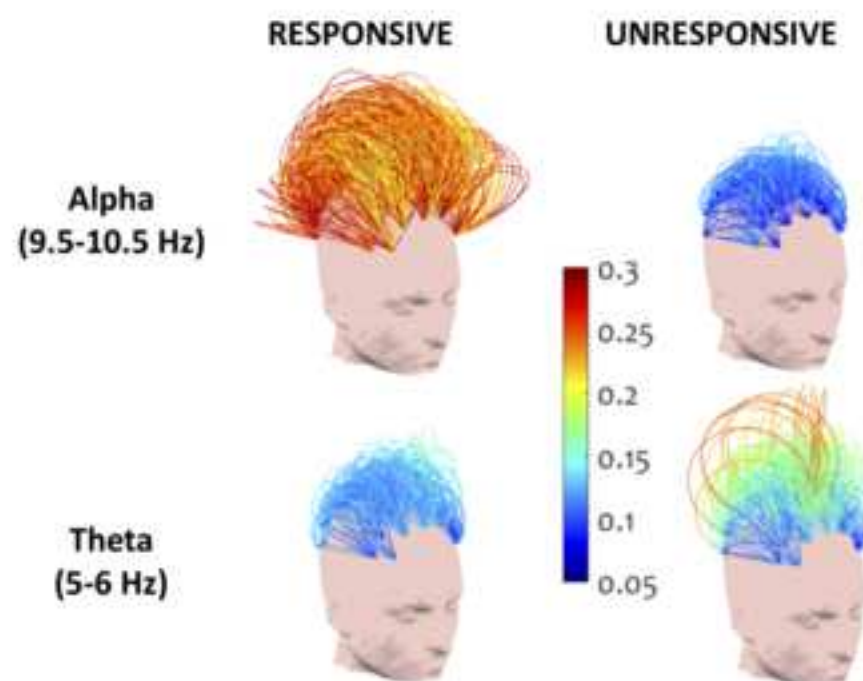
Reaction times (s) and data selection

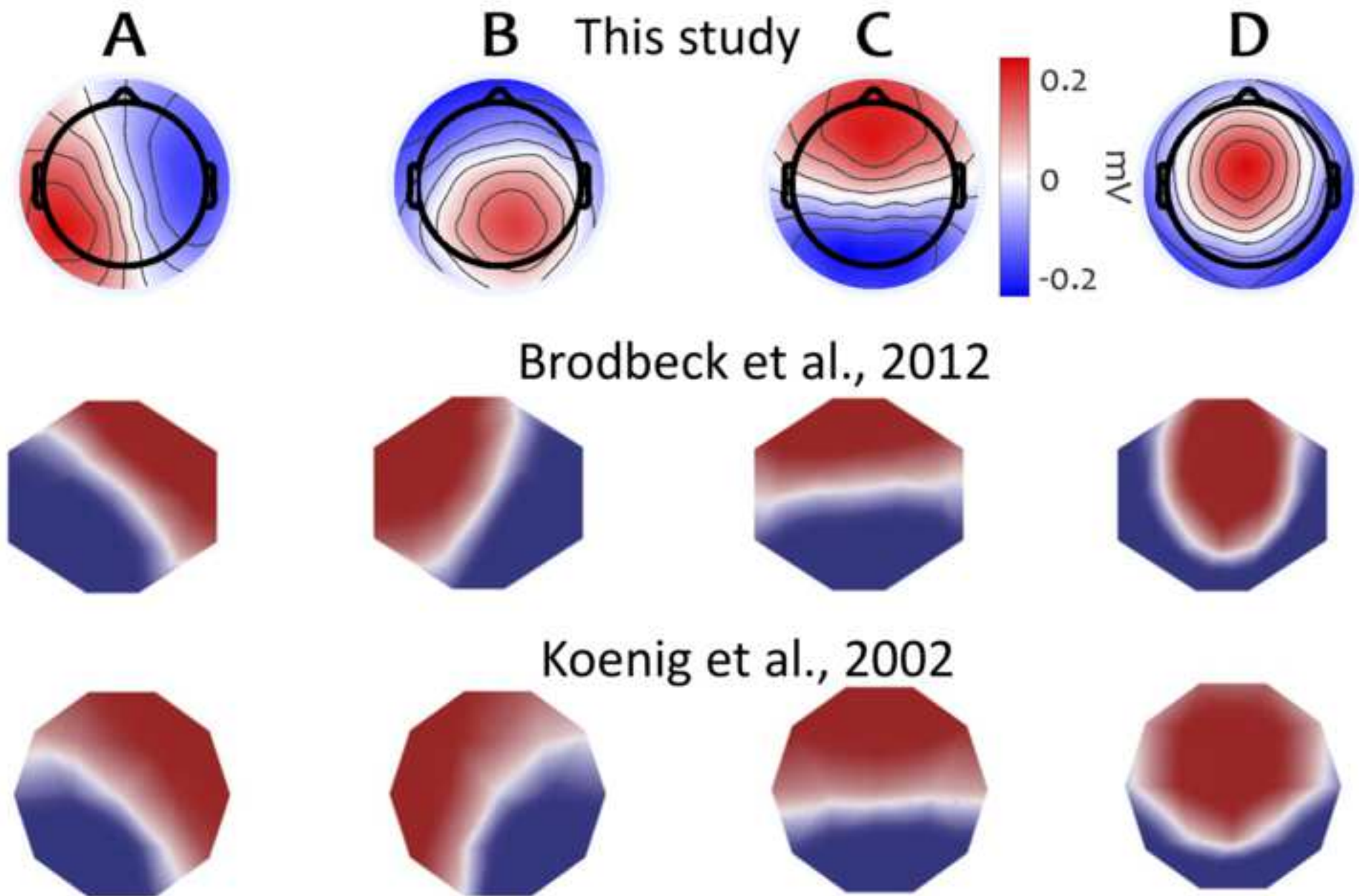


A. Spectral power contribution



B. Frontoparietal WPLI connectivity





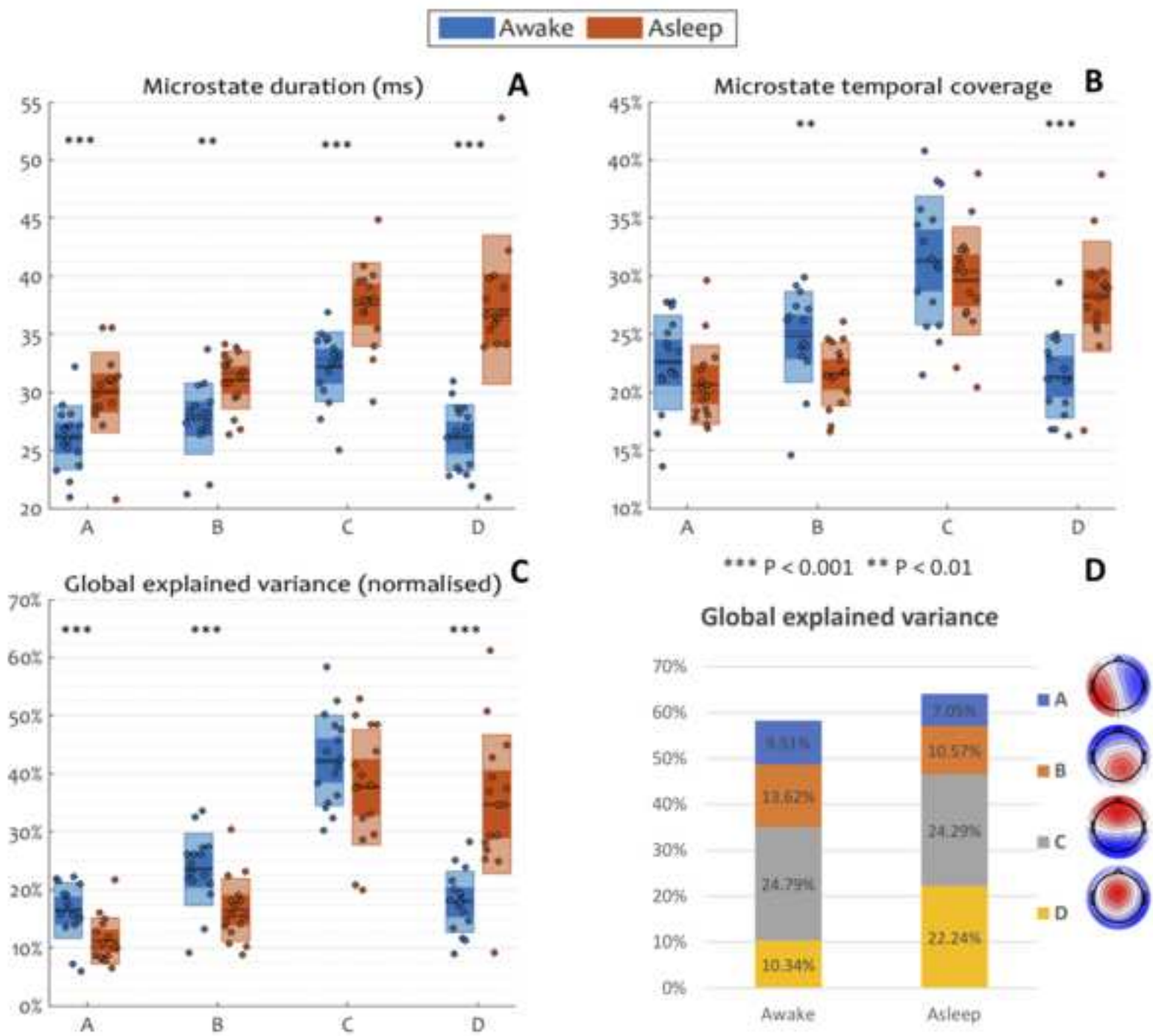
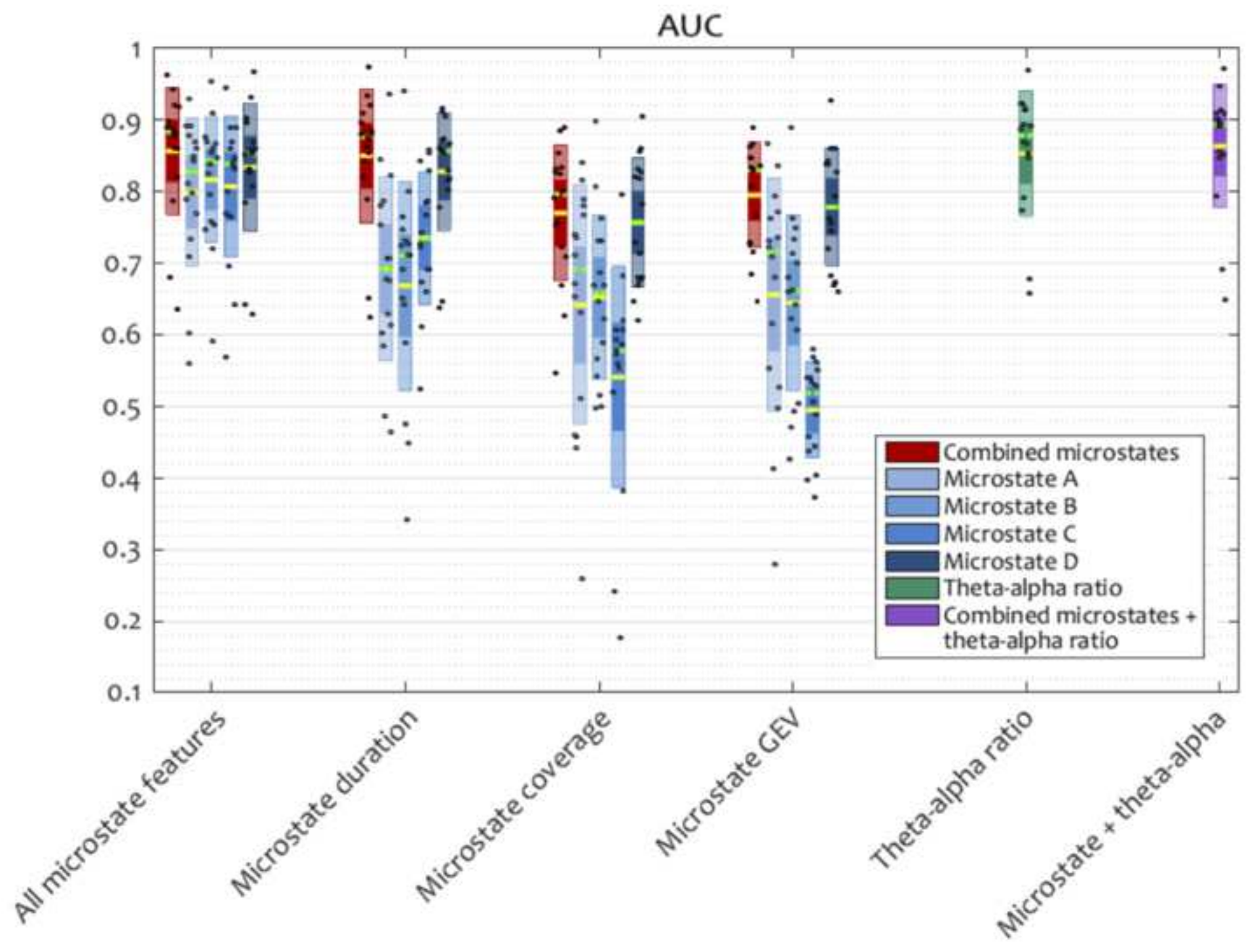
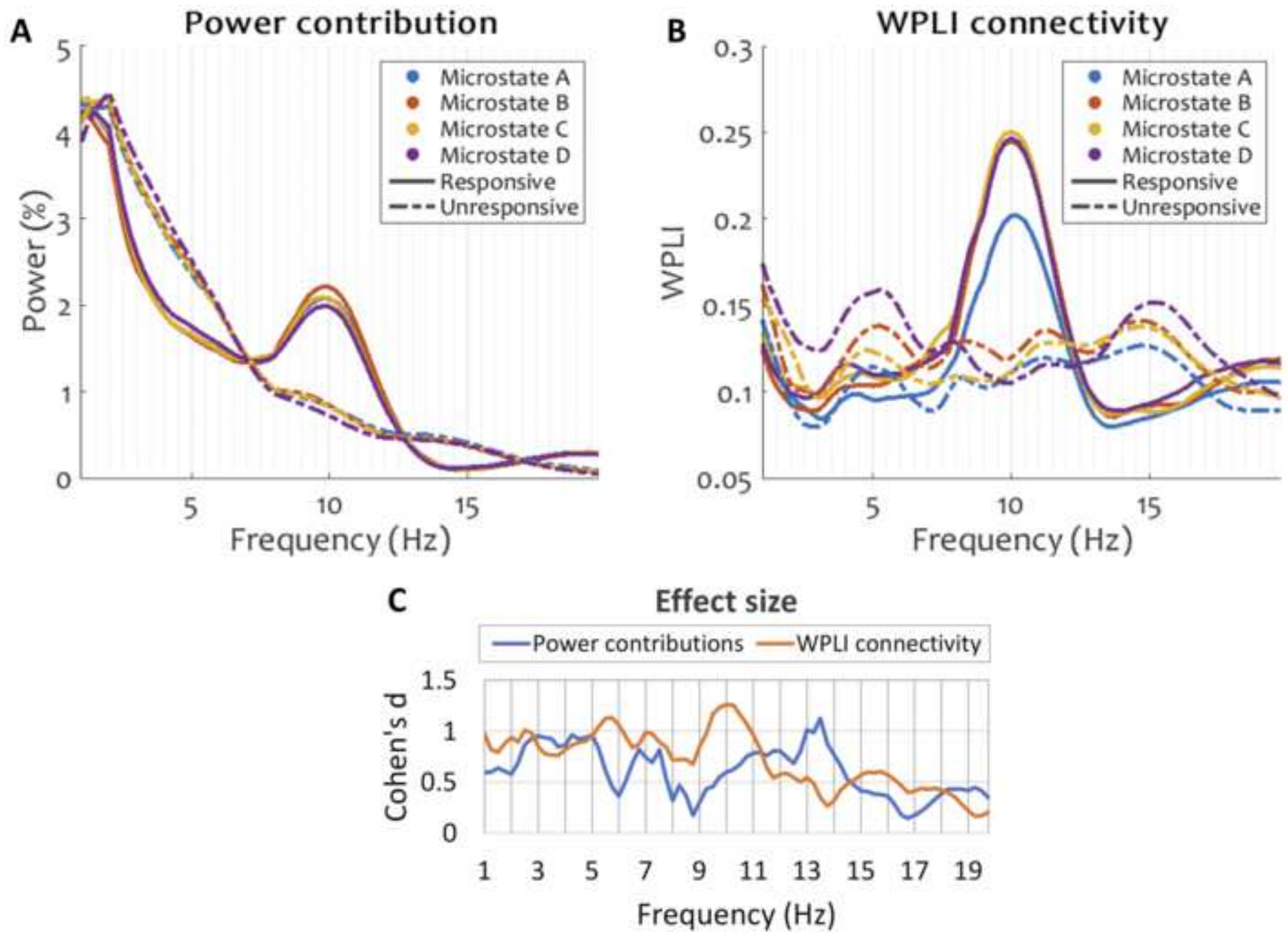
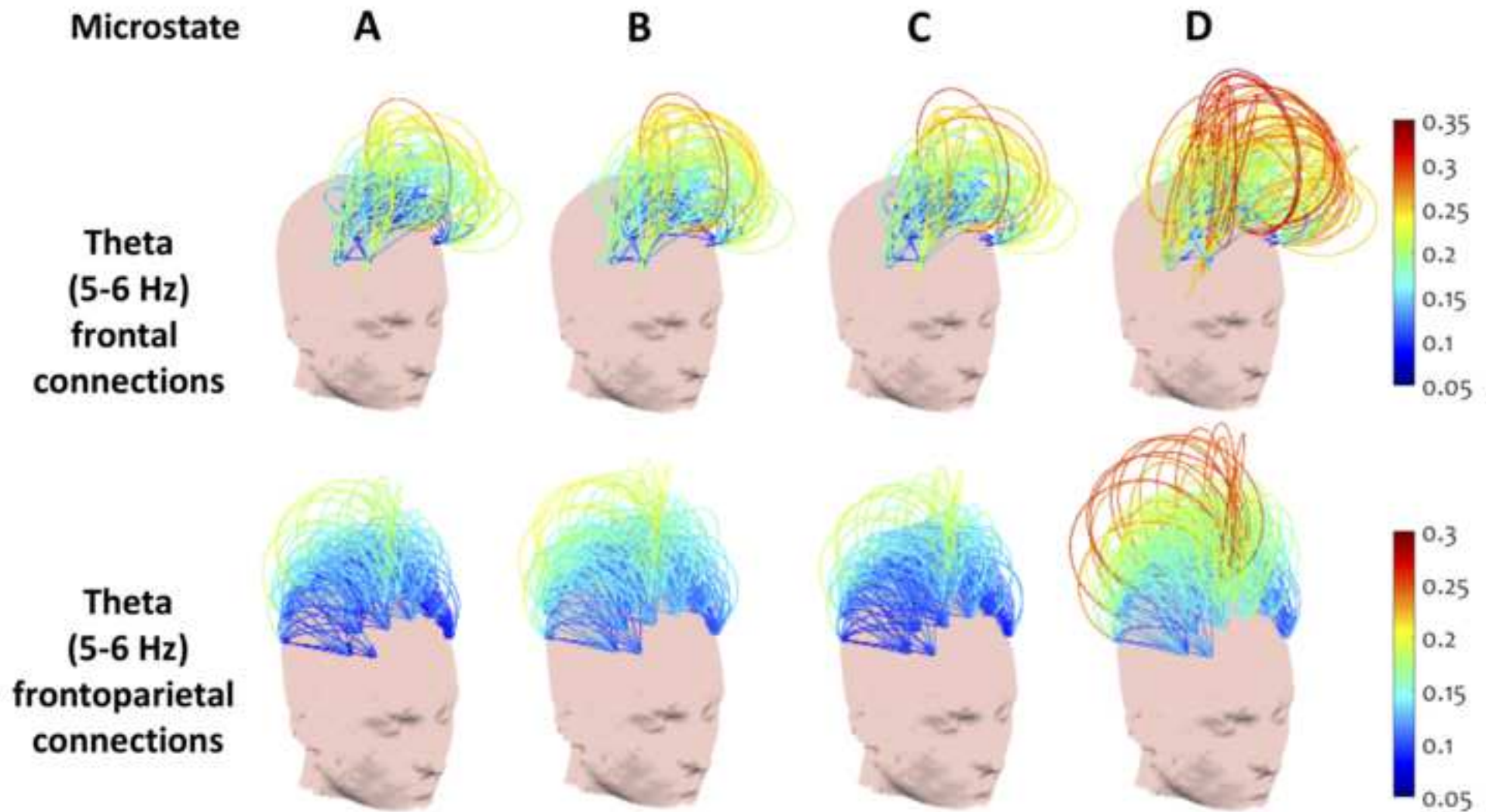


Figure 5

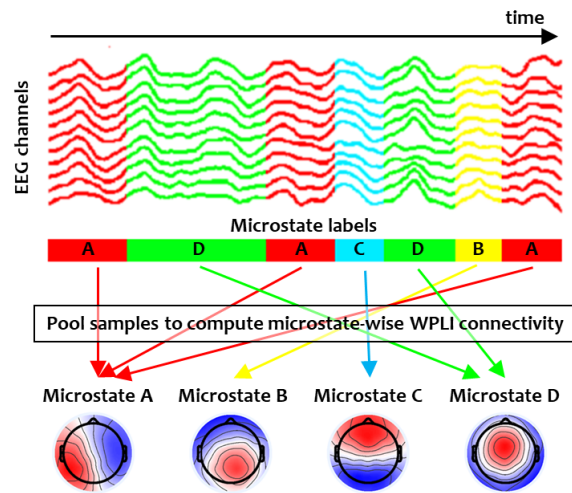




WPLI connectivity during unresponsiveness



1 Supplementary Material

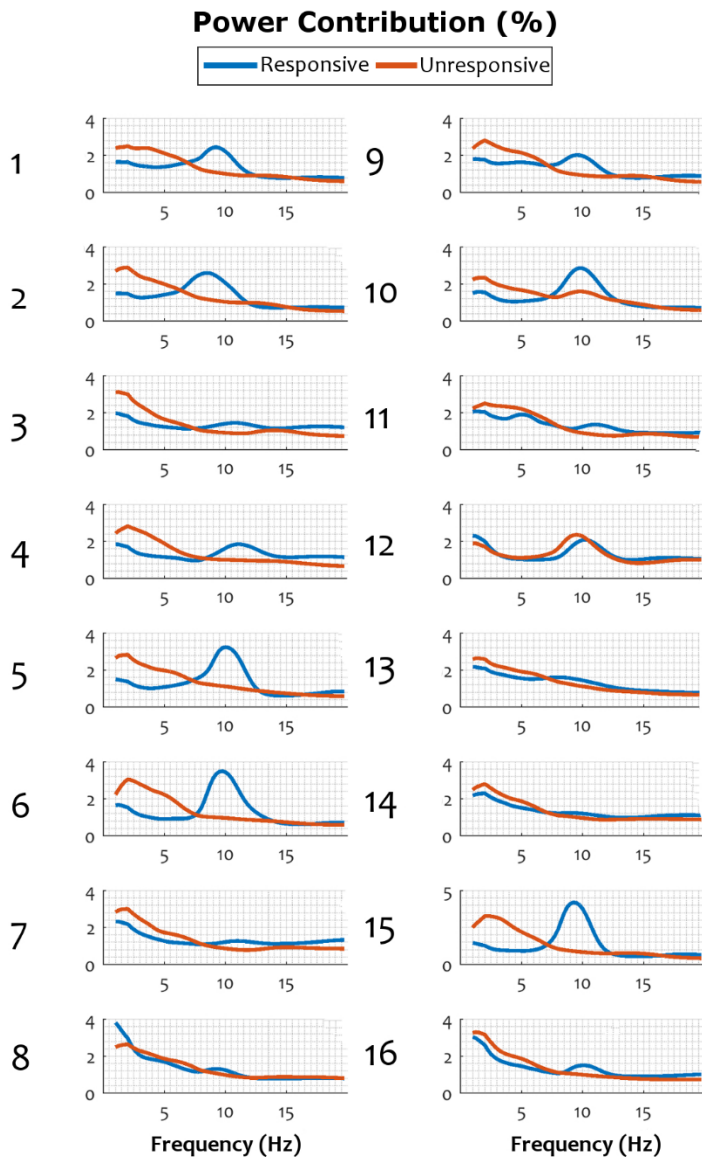


2

3 **Supplementary Figure 1. Computation of microstate-wise WPLI connectivity.** Instantaneous channel-wise
4 Hilbert estimates of phase angle at each time sample were pooled together according to the microstate label
5 assigned to the sample. For each microstate, the pooled Hilbert phase angles at each channel were then used
6 to compute WPLI between pairs of channels.

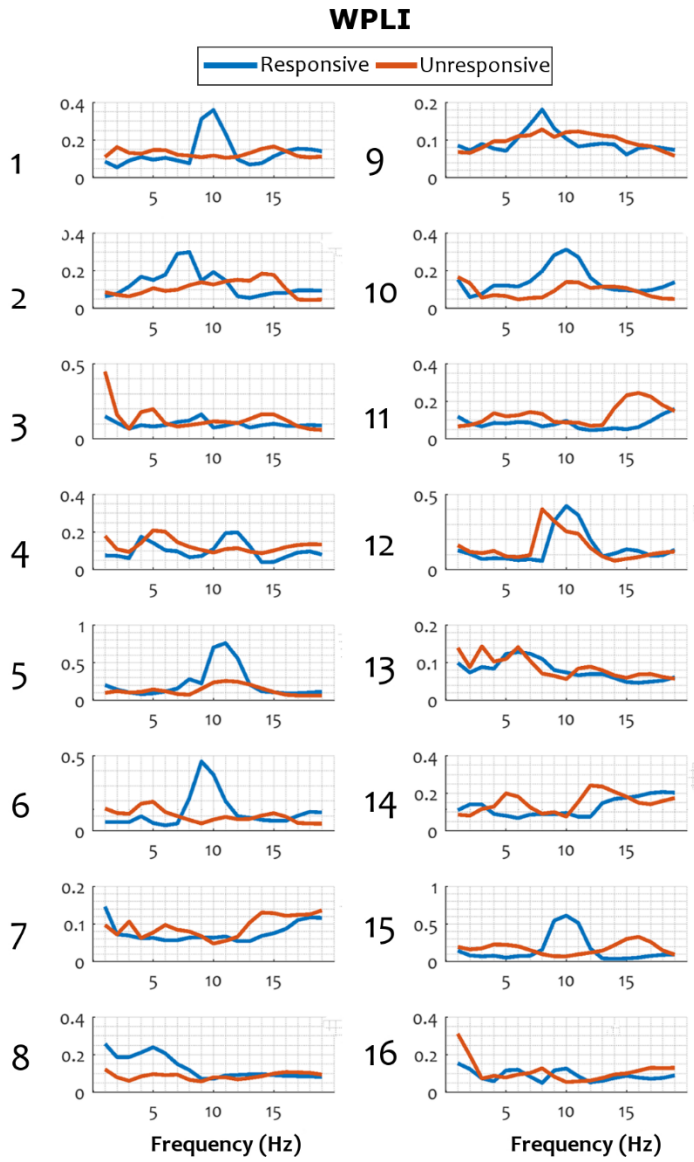
7

8



9

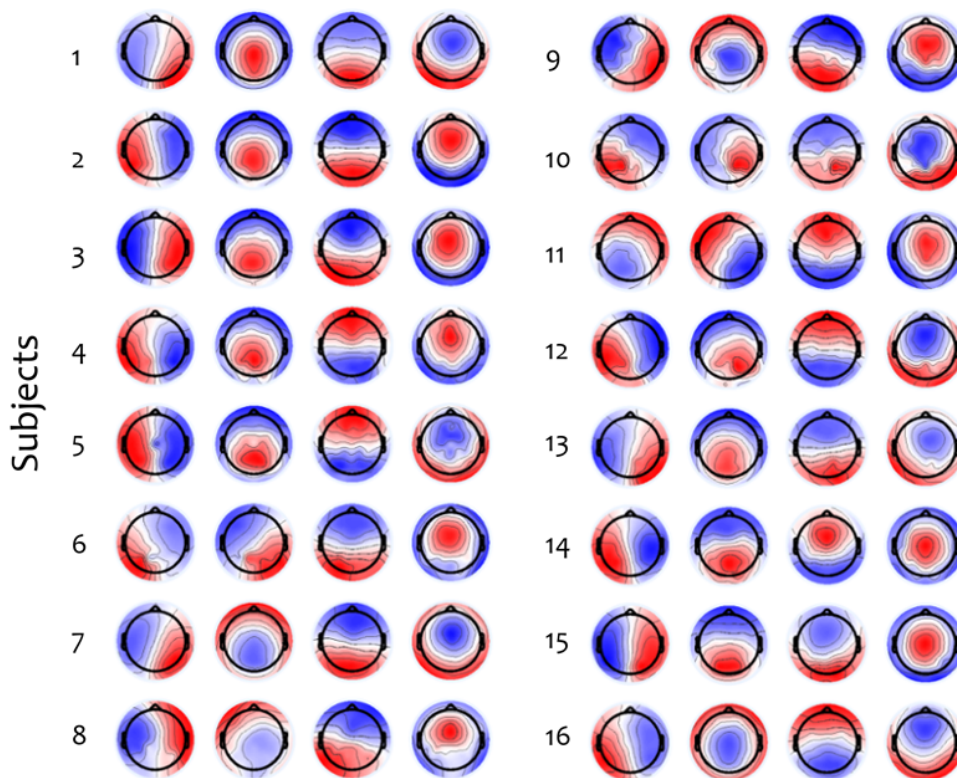
10 **Supplementary Figure 2. Individual subject spectral power contributions before and after loss of**
 11 **responsiveness.** For each subject, values are averaged over posterior channels (see main text).



12

13 **Supplementary Figure 3. Median WPLI before and after loss of responsiveness in individual subjects. WPLI**

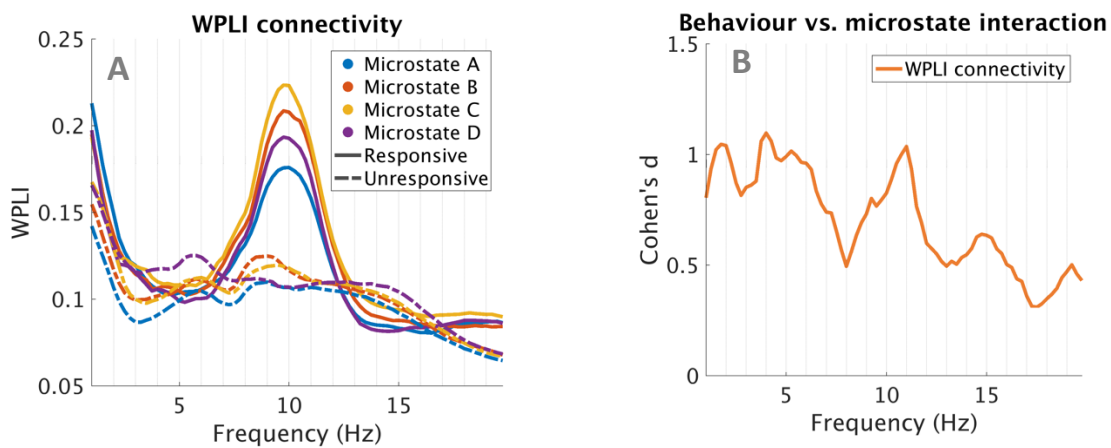
14 values are averaged across all channel pairs.



15

16 **Supplementary Figure 4. Microstate topographies in each subject, computed over the responsive and**
 17 **unresponsive periods.** In each subject, maps are ordered such that they have maximal spatial correlation with
 18 corresponding group-level maps in Fig. 3, ignoring map polarity.

19



20 **Supplementary Figure 5. WPLI connectivity and interaction effect size after Current Source Density**
 21 **Estimation.** Panels A and B re-plot Figs. 6B and 6C after re-estimating WPLI calculated with current source
 22 density estimates.